芝浦工業大學
SHIBAURA INSTITUTE OF TECHNOLOGY

Gait-Behavior Optimization Considering Arm Swing and Toe Mechanisms for Biped Robot on Rough Road

Author:
NGUYEN VAN TINH
Student ID: NB16508

Supervisor:
Professor. Dr. Eng.
HIROSHI HASEGAWA

A DISSERTATION SUBMITTED IN PARTIAL FULFILLMENT OF THE REQUIREMENTS FOR THE DEGREE OF

DOCTOR OF PHILOSOPHY

September, 2019

Declaration of Authorship

- This work was done wholly or mainly while in candidature for a research degree at this University.
- Where any part of this thesis has previously been submitted for a degree or any other qualification at this University or any other institution, this has been clearly stated.
- Where I have consulted the published work of others, this is always clearly attributed.
- Where I have quoted from the work of others, the source is always given. With the exception of such quotations, this thesis is entirely my own work.
- I have acknowledged all main sources of help.
- Where the thesis is based on work done by myself jointly with others, I have made clear exactly what was done by others and what I have contributed myself.

Signed:

_____

Date:

_____

Abstract

This research addresses a gait generation approach for the biped robot which is based on considering that a gait pattern generation is an optimization problem with constraints where to build up it, Response Surface Model (RSM) is used to approximate objective and constraint function, afterwards, Improved Self-Adaptive Differential Evolution Algorithm (ISADE) is applied to find out the optimal gait pattern for the robot. In addition, to enhance stability of walking behavior, I apply a foot structure with toe mechanism. This is to enable the robot to overcome the challenge on uneven terrain. Arm swinging mechanism is also considered to restrict rotation of the robot during locomotion. Finally, to evaluate the achievement of this research, the result is validated through dynamic simulation on a commercially available software called Adams (MSC software, USA) with the model which is designed by referring to KHR-3HV robot, belongings to Kondo Kagaku company. The robot posture is comparable to the human in a cycle of the walking process. As a result, I confirmed that the approximated optimization method by applying ISADE algorithm and RSM is an effective approach to generate a gait pattern for the robot. With generated gait, the robot can walk steadily on flat ground and overcomes obstacle on rough road. Toe mechanism enhances ability of the robot while climbing up uneven segment of rough terrain and arm swing mechanism reduces angle of rotation in motion.

Acknowledgements

Firstly, I would like to express my sincere gratitude to my advisor Prof. Hiroshi Hasegawa for the continuous support of my study and related research, for his patience, motivation, and immense knowledge. His guidance helped me in all the time of research and writing of this thesis.

Last but not the least, I would like to thank my parents and my friends for supporting me spiritually throughout doing this research and my life.

Contents

List of Figures

List of Tables

Nomenclature

Notation

ADAMS Automated Dynamic Analysis of Mechanical Systems.

ANN Artificial neural network.

ANOVA Analysis of variance.

CoM Center of mass.

CPG Central pattern generator.

DE Differential evolution.

DoE Design of experiment.

DoF Degrees of freedom.

EAs Evolutionary algorithms.

FEM Finite element method.

ISADE Improve self-adaptive differential evolution.

LR Loading response.

MSt Mid stance.

PSw Pre-swing.

RSM Response surface model.

SA Simulated annealing.

TSt Terminal stance.

ZMP Zero moment point.

Greek symbols

γ Penalty coefficient.

ω Angular velocity.

φ_i Angle of *i* joint.

Sets

$V_{i,j}^G$ j^{th} element of mutant vector V_i^G.

V_i^G Mutant vector in DE.

R_f Angle of rotation.

X_f Lateral distance.

Y_f Distance from CoM to ground.

Z_f Walking distance.

a_p, b_p, c_p, d_p Coefficient of RSM function.

a, b, c, d Coefficient of gait function.

N Number of simulation steps.

n Number of variables.

t Time.

Chapter 1

Introduction and Objectives

This chapter starts out by introduction to humanoid robot and a survey of related research. Then, challenges and objective of this dissertation are discussed. The end of this chapter presents the outline of its organization.

1.1 Introduction to Biped Robot

The word "robot" comes from "robota" in Czech language. This word, which from "Rossum's Universal Robots" (R.U.R.) produced by Kalvel Capek in 1920, means work as slave or forced worker. This plot is renowned and the word "robot" is very popular all over the world. The performance is related to human's imagination that tries to find something for serving responsibilities. The robot manufacturing originates from this idea.

A biped or humanoid robot is a robot with its body shape built to resemble the human body. The design may be for functional purposes, such as interacting with human tools and environments, for experimental purposes, such as the study of bipedal locomotion, or for other purposes. In general, humanoid robots have a torso, a head, two arms, and two legs, though some forms of humanoid robots may model only part of the body, for example, from the waist up. Some humanoid robots also have heads designed to replicate human facial features such as eyes and mouths.

Purpose: Humanoid robots are now used as research tools in several scientific areas. Researchers study the human body structure and behavior to build humanoid robots. On the other side, the attempt to simulate the human body leads to a better understanding of it. Human cognition is a field of study which is focused on how humans learn from sensory information in order to acquire perceptual and motor skills. This knowledge is used to develop computational models of human behavior and it has been improving over time.

It has been suggested that very advanced robotics will facilitate the enhancement of ordinary humans.

Although the initial aim of humanoid research was to build better orthosis and prosthesis for human beings, knowledge has been transferred between both disciplines. A few examples are powered leg prosthesis for neuromuscularly impaired, ankle-foot orthosis, biological realistic leg prosthesis and forearm prosthesis.

Besides the research, humanoid robots are being developed to perform human tasks like personal assistance, through which they should be able to assist the sick and elderly, and dirty or dangerous jobs. Humanoids are also suitable for some procedurally-based vocations, such as reception-desk administrators and automotive manufacturing line workers. In essence, since they can use tools and operate equipment and vehicles designed for the human form, humanoids could theoretically perform any task a human being can, so long as they have the proper software. However, the complexity of doing so is immense.

They are also becoming increasingly popular as entertainers. For example, Ursula, a female robot, sings, plays music, dances and speaks to her audiences at Universal Studios. Several Disney theme park shows utilize animatronic robots that look, move and speak much like human beings. Although these robots look realistic, they have no cognition or physical autonomy. Various humanoid robots and their possible applications in daily life are featured in an independent documentary film called *Plug & Pray*, which was released in 2010.

Humanoid robots, especially those with artificial intelligence algorithms, could be useful for future dangerous and/or distant space exploration missions, without having the need to turn back around again and return to Earth once the mission is completed [1].

1.2 Theories of Walking

1.2.1 Gait cycle

A gait cycle is the time period or sequence of events or movements during locomotion in which one foot contacts the ground to when that same foot again contacts the ground, and involves forward propulsion of the centre of gravity. A single gait cycle is also known as a stride [2]. The walking process has cycle or gait cycle that can be presented as Fig. 1.1.

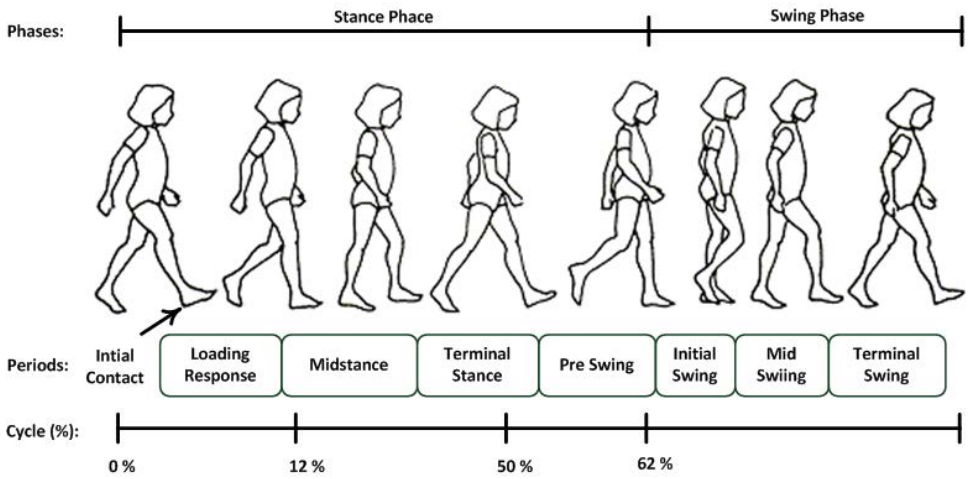

FIGURE 1.1: Phases of the nomal gait cycle [3].

Each gait cycle or stride has two phases as below [4]:

Stance Phase: The stance phase is that part of a gait cycle during which the foot remains in contact with the ground. For analysing gait cycle one foot is taken as

reference and the movements of the reference foot are studied. It constitutes of 60% of the gait cycle. In stance phase the reference foot undergoes five movements:

- Initial Contact (Heel Strike): In initial contact, the heel is the first bone of the reference foot to touch the ground.
- Loading Response (Foot Flat): In loading response phase, the weight is transferred onto the referenced leg. It is important for weight-bearing, shock-absorption and forward progression.
- Mid Stance: It involves alignment and balancing of body weight on the reference foot.
- Terminal Stance: In this phase the heel of reference foot rises while the its toe is still in contact with the ground.
- Toe Off (Pre Swing): In this phase, the toe of reference foot rises and swings in air. This is the beginning of the swing phase of the gait cycle.

Swing Phase: The swing phase is that part of the gait cycle during which the reference foot is not in contact with the ground and swings in the air. It constitutes about 40% of gait cycle. It has three parts:

- Initial Swing: This first phase is approximately one-third of the swing period. It begins with lift of the foot from the floor and ends when the swinging foot is opposite the stance foot.
- Mid Swing: The second phase of the swing period begins as the swinging limb is opposite the stance limb. The phase ends when the swinging limb is forward and the tibia is vertical
- Terminal Swing: This final phase of swing begins with a vertical tibia and ends when the foot strikes the floor. Limb advancement is completed as the leg moves ahead of thigh

1.2.2 ZMP and support polygon

Definition of ZMP In 1972, Vukobratović and Stepanenko defined the Zero-Moment Point (ZMP) at the beginning of the paper on control of humanoid robots. Everything of the argument regarding the ZMP starts from here.

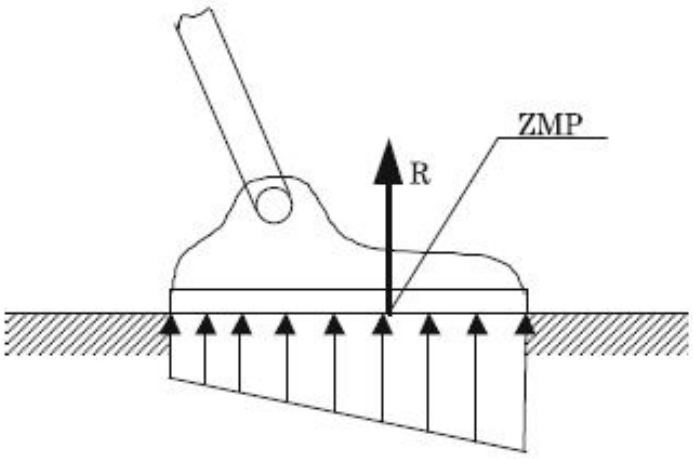

FIGURE 1.2: Definition of Zero-Moment Point (ZMP) [5].

In Fig. 1.2 an example of force distribution across the foot is given. As the load has the same sign all over the surface, it can be reduced to the resultant force R, the point of attack of which will be in the boundaries of the foot. Let the point on the surface of the foot, where the resultant R passed, be denoted as the zero-moment point, or ZMP in short.

ZMP and support polygon the support polygon which is another important concept related to the ZMP. As shown in Fig. 1.3, let us consider the region formed by enclosing all the contact points between the robot and the ground by using an elastic cord braid. We call this region as the support polygon. Mathematically the support polygon is defined as a convex hull, which is the smallest convex set including all contact points. Definitions of the convex set and the convex hull are explained in the appendix of this chapter. Rather than detailed discussions, I first show a simple and

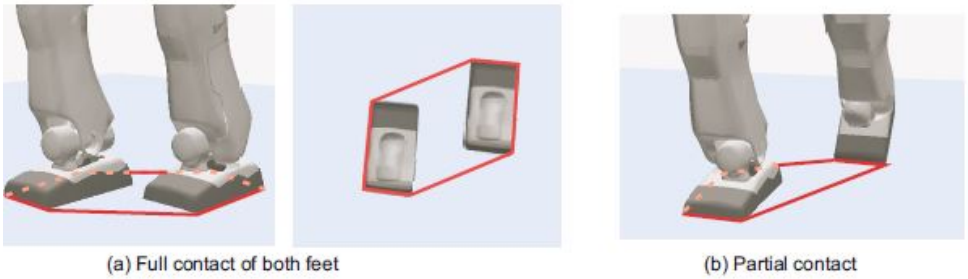

FIGURE 1.3: Support polygon [6].

important relationship between the ZMP and the support polygon. *The ZMP always exists inside of the support polygon*.

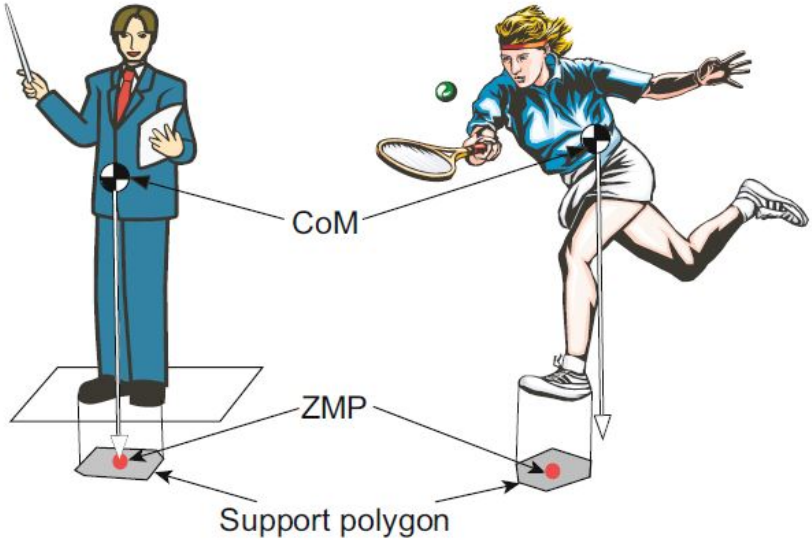

FIGURE 1.4: CoG, ZMP, and support polygon [6].

Figure 1.4 illustrates the relationship among the center of mass (CoM), ZMP and the support polygon while a human stands on the ground. When a human stands on the ground, the ZMP coincides with the ground projection of CoM. In such a case, a human can keep balance if the ground projection of CoM is included strictly inside of the support polygon. On the other hand, when a human moves dynamically, the ground projection of CoM may exist outside the support polygon. However, the

ZMP never exists outside the support polygon.

1.3 Human foot

1.3.1 Anatomy

In the walking process of human, toes which help the contact between feet and ground smoothly, have an important role in walking stability. The foot is a very complicated structure as described in Fig. 1.5, which is best thought of as being in three parts [7]:

- The *hindfoot* , which consists of two bones, one on top of the other.
- The *midfoot*, which consists of five bones, packed closely together.
- The *forefoot*, which consists of the five metatarsals and the toes.

The talus or astragalus is the upper of the two bones in the hindfoot. Its superior surface forms the ankle joint, articulating above and medially with the tibia and laterally with the fibula. Below, the talus articulates with the calcaneus through the subtalar joint. It articulates anteriorly with the most medial and superior of the midfoot bones - the navicular.

The calcaneus or os calcis lies below the talus and articulates with it through the subtalar joint. Its lower surface transmits the body weight to the ground through a thick layer of fat, fibrous tissue and skin - the heelpad. The anterior surface articulates with the most lateral and inferior of the midfoot bones - the cuboid. The midfoot consists of five bones: The five metatarsals lie roughly parallel to each other, the lateral two articulating with the cuboid and the medial three with the three cuneiform bones. The phalanges are the bones of the toes; there are two in the big toe and three in each of the other toes. The big toe is also called the great toe or hallux. A joint occurs where one bone is in contact with another. From a practical point

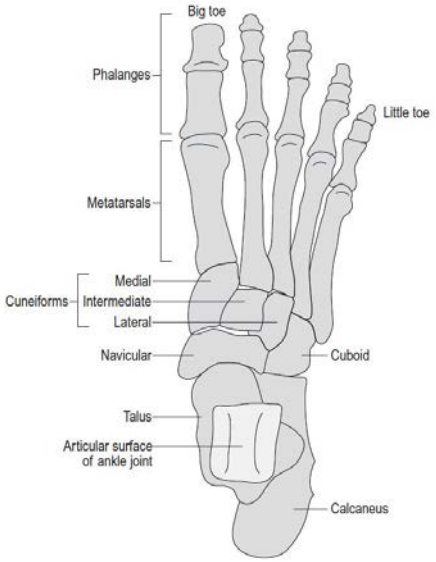

FIGURE 1.5: Human right foot structure [7].

of view, they can be divided into synovial joints, in which significant movement can take place, and the various other types of joint in which only small movements can occur. Since gait analysis is normally only concerned with fairly large movements, the description which follows deals only with synovial joints. In a synovial joint, the bone ends are covered in cartilage and the joint is surrounded by a synovial capsule, which secretes the lubricant synovial fluid. Most joints are stabilized by ligaments, which are bands of relatively inelastic fibrous tissue connecting one bone to another. Fascia is a special type of ligament, being a continuous sheet of fibrous tissue.

1.3.2 Relationship between Gait Phases and Foot Pressure Patterns

In normal barefoot walking, the heel was the first portion of the foot to receive body weight followed by midfoot and forefoot, finally the load shifted to the toe for lift off as shown in Fig. 1.6

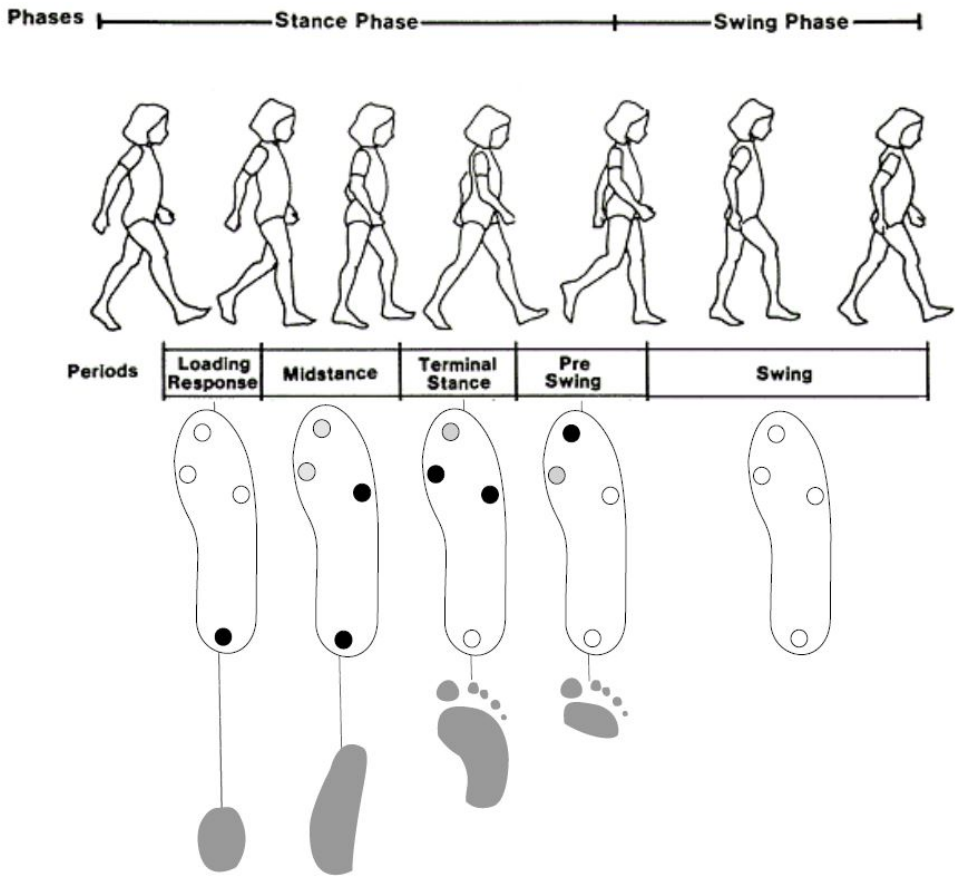

FIGURE 1.6: Foot pressure pattern [8].

Figure 1.6 represents the expected pressure patterns in each stance subphase (LR, MSt, TSt, PSw). The black area is the position where supports forces areas. Wherewith, LR is heel only in loading response, MSt is foot flat in mid stance, TSt is forefoot and toes in terminal stance, and PSw is medial forefoot in pre-swing. When the load from body sends to the foot, the force will goes through plantar tissues. The force has the stability related to the intensity of the loading force and the area of the foot in contact with the floor [4].

- Heel pressure shows two patterns. Initial loading occurs on a small posterior lateral area, and body weight is dropped rapidly. All total force, ranging between 70% and 100% of body weight.

- Advancement of body weight onto the center of the heel reduces the pressures to a third (33% of body weight)
- Lateral mid foot contact with the floor is moderately common but of low intensity. The pressure in this area averages 10% of body weight.
- Metatarsal head pressure differs among the individual bones. Generally the highest pressures are registered under the second and third metatarsal heads. Whether the forces are equal or one is slightly greater than the other is highly variable among individuals. Compared to the posterior heel value, the metatarsal head pressures varied between 60% and 100% of body weight.
- Toe pressures differ markedly. The hallux (bigtoe) has the greatest pressure. It ranged between 30% and 55% of that at the heel. The fifth metatarsal head always registered the least pressure within the forefoot.

1.4 Previous highlight research on Biped Robot

The researches of humanoid robot and biped robot have a long history and continuation in two decades. In order that the robot has capable of gestures, expressions, replicates, and decisions human-like. The researches of biped robot have spread extensively and have been extremely favorite topic. On account of, all of these respond to human needs in industries, services and entertainments. Because of these reasons, the studies of robot are popular. One of the important researches and very basic mobility is walking. This is proved by the medical research about the human gait that has been continuously as with the gait of biped robot.

For two decades, the studies of walking biped robot are incessant research topic such as ASIMO, WABIAN-2, WABIAN-2R, HRP2, HRP3, HRP4C, H6 and H7 etc. Let me divide these robot into two groups.

Universities and Research Institutes In Japan, professor Takanishi's group in Waseda University has been actively developing many biped robots such as WABIAN-2, WABIAN-2R [10, 11] following professor Kato who built world's fist humanoid robot WABOT-1. The WABIAN-2 has been designed according to a development of robot having capability of walking like humans walking. WABIAN-2 can obtain data needed for developing medical and rehabilitation instruments by measuring the robot's motions instead of a human, which are difficult to measure quantitatively. WABIAN-2 has capable of walking without the bent knee posture that different from among common bipedal humanoid robots because it has added degrees of freedom in its rocking waist, swiveling knees, and pivoting ankles. In 2006, WABIAN-2R was developed for two purposes. The first one is to develop a robot that would be a human's partner. The second one is to develop a human motion simulator. WABIAN-2R has been designed mimic human movements, the robot has 41 DOFs and the movable range of the joints is designed reference from human. WABIAN-2R used a photo sensor to detect the basing angle. Also, each ankle has a 6-axis force/torque sensor, which is used for measuring Ground Reaction Force (GRF) and Zero Moment Point (ZMP). In the feet part, WABIAN-2R's foot is designed to be similar to human foot. A Foot with a passive toe joint is applied with WABIAN-2R, this application based on the results of gait analysis with motion capture system. Researchers focus on a walking steady, they offer these main advantages because it lightweight and don't need a necessity complex control structure. In addition, one of the human walk characteristics is heel-contact and toe-off motions in steady walking. From the reasons, the researchers have developed the principle of the pattern generation for stretched knee, heel-contact and toe-off motions. This development based on the ZMP criterion applied with WABIAN-2R. For the pattern generation, some parameters of the foot trajectories of a biped robot were optimized by using a genetic algorithm in order to generate a continuous and smooth motion of leg. The results obtained from WABIAN- 2R have the ability to realize more human-like

walking styles. The development of the robot's feet is continuous study. In 2009, foot with human-like arch structure was presented. The researchers described a new foot mechanism composed of mimicking the human's foot arch structure and the function of the arch structure. The developed foot mimics the elastic properties of the arch of human's foot and the change of arch height during walking. The foot mechanism consists of a passive joint in the internal toe, a passive joint in the external toe, and joint in the foot arch. The result of arch elasticity shown that it could absorb a foot-landing force at the plantar contact phase and the change of the arch height contributed to a strong trust at the push-off phase. In 2010, WABIAN-2R is capable of two walking styles, one is knee-stretched walking like a human, another one is knee-bend walking. Knee-stretched walking enables fast walking. In contrast, kneebend walking enables stable walking on uneven terrain. In the real environment, it is preferable that WABIAN-2R change the walking style depending on the ground condition. WABIAN-2R researchers developed a new inverse kinematics method to generate walking motions of robot legs regardless of the walking style and an online walking parameter generation to bend its knees depending on the ground condition. By using the methods and the online pattern generation method above, an adaptive walking process was realized. Design and development capabilities as mention above, these are some of the WABIAN-2R researches.

ATR Computational Neuroscience Laboratories is studying humanoid robots from a viewpoint of brain science. Using the humanoid robot CB-i developed by SARCOS Inc., their biologically feasible balance controller has been tested [12].

Needless to say, biped humanoid research is not limited in Japan. As remarkable examples, we can see LOLA by Technische Universität of München (TUM) [13], HUBO2 by Korea Advanced Institute of Science and Technology (KAIST) [14], BHR-2 by Beijing Institute of Technology [15], iCub by Italian Institute of Technology (IIT), the University of Genoa [16], CHARLI by Virginia Polytechnic Institute and State University [17], and TORO by the German Aerospace Center (DLR) [18, 19].

FIGURE 1.7: WABIAN-2R humanoid robot.

Companies ASIMO of HONDA [9] is undeniable that the launch of ASIMO cause excitement and increase in the study of biped robot's popularity. ASIMO has been developed from Honda P-series bipedal robot (P1, P2, and P3) until it has small and lightweight. ASIMO has many abilities such as to run, walk smoothly, climb stairs, and communicate human-like. The controller that controls ASIMO's movement is housed in the robot's waist area and can be controlled by a PC or wireless controller. The fact that human has toes for helping our body balance was also taken into consideration. The ASIMO's posture actually has soft projections on its feet that play a similar role to the one of human toes play when human walk. This soft material also absorbs impact on the joints, just as our soft tissues do when human walk. ASIMO has 34 degrees of freedom totally including six on each leg spread over different points of its body in order to allow it to move freely. The number of degrees of freedom was necessary variable for ASIMO's legs and they were designed by measuring human joint movement while walking on flat ground, climbing stairs and running.

ASIMO's engineers had to find a way to work with the inertial forces created while walking. This is called the "zero moment point" (ZMP). ZMP is defined as the point on the ground at which the net moment of the inertial forces and the gravity forces has no component along the horizontal axes. To control ASIMO's posture, engineers worked on three areas of control: First, floor reaction control means regulation the soles of the feet absorb floor unevenness while still maintaining a firm stance. Second, target ZMP control means the control state that ASIMO can't stand firmly and its body begins to fall forward, the controller maintains position by moving its upper body in the opposite direction to the impending fall. At the same time, it increases walking speeds quickly to counterbalance the fall. Third, Foot-planting location control is used when the target ZMP control has been activated. The controller adjusts the length of the step to regain the right relationship between the position and speed of the body. The success of the control system is that the ASIMO's posture is widely studied and applied to the walking robot field.

FIGURE 1.8: ASIMO humanoid robot.

The QRIO was a bipedal humanoid entertainment robot developed and manufactured by Sony Intelligence Dynamics Laboratory, Inc [20]. QRIO is capable of voice and face recognition, making it able to remember people as well as their likes and dislikes. A video on QRIO's website shows it speaking with several children. QRIO stood approximately 0.6 m tall and weighed 7.3 kg. It can run at 23 cm/s.

FIGURE 1.9: QRIO humanoid robot.

Kawada Industries Inc. launched on the development of humanoid robots involved in H6 and H7 [21, 22] projects of the University of Tokyo. H6 has 1370 mm height, and its mass is 55 kg including 4 kg of batteries. H6 is designed as a research platform of the humanoid robot that can interact to the complex environment by coupling sensor and behavior. H7 is designed to be a human-sized robot capable of operating autonomously in indoor environments for humans. H7 has 1470 mm height, and the mass is 58 kg. It has 35 DOF totally. Researchers have developed an efficient walking trajectory generation method that follows a given input ZMP trajectory for H7. The key to our method is the modification of the torso horizontal trajectory from a given initial trajectory, by using dynamic trajectory generation and

motion planning control software. Therefore, H7 can walk up and down 25 cm high steps.

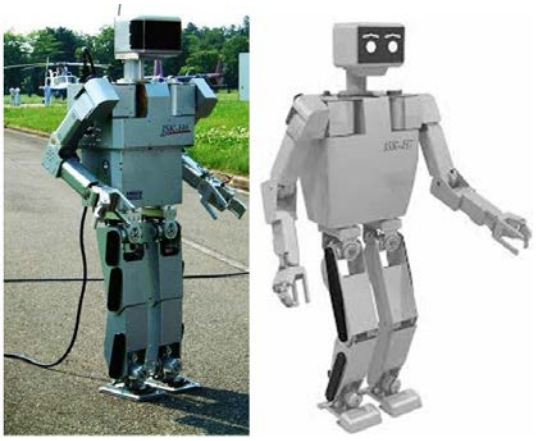

FIGURE 1.10: H6 (left) and H7 (right) humanoid robots.

(A) (B) (C)

FIGURE 1.11: Humanoid robot: (a) HRP-2; (b) HRP-3; and, (c) HRP-4.

In addition, Kawada Industries has attended the Humanoid Robotics Project (HRP) of the Ministry of Economy, Trade and Industries of the Japanese Government (METI). They had developed HRP-2 [23], HRP-3 [24], HRP-4 [25] and HRP-4C [26]. The objective of this project is to develop a safe, reliable, and human-friendly robot

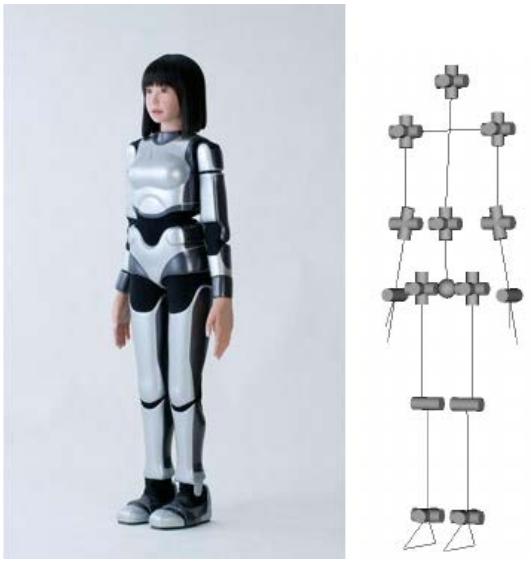

FIGURE 1.12: HRP-4C humanoid robots.

system. The developed robot has an ability to carry out complicated tasks and supporting humans within human living and working environments. HRP-2 is the final robotic platform for the HRP together with the Humanoid Research Group of National Institute of Advanced Industrial Science and Technology (AIST), and Yaskawa Electric Corporation. HRP-2 has an ability to walk on narrow paths, to cope with uneven surface, to walk at two third level of human speed, to lie down, and to get up by a humanoid robot own self. It has a body similar to human's body by eliminating a backpack for electronics installation. HRP-3, which is developed subsequently, is a model with strong focus on operating under severe outdoor environments. HRP-3 is capable not only of operating in rain, but also of walking on a slippery floor surface. To control of legged locomotion, HRP-3 researchers used ZMP concept, which can be utilized for calculating the stability criterion even if contact points between a humanoid robot and environment doesn't exist in the same plane. HRP-4 is presented in 2011 with expectation that it will accelerate the R&D of next-generation robot systems necessary for the robot industry of the future, which is expected to be human-cooperative and capable of operating under various environments. HRP-4C

announced in 2009, it is a female humanoid robot with an appearance exactly like a human. She has been named "Miim". This robot has 158 cm height and 46 kg weight. HRP-4C is being developed for the entertainment industry. For characteristics of the legs, HRP-4C's knees are stretched by up/down motion of the waist, she mimics the swing motion of human legs, and the single-toe supporting realizes longer strides. The foot of HRP-4C used active toe joint for realizing human-like walking motion. In addition, the hand was redesigned to realize a human-size with realistic skin, also the eye with camera provides visible and useful image for operation and color recognition without deviation from human appearance. HRP-4C became a global focus of interest immediately after its announcement.

In 2009, Boston Dynamics unveiled the Protection Ensemble Test Mannequin (PETMAN) which is a humanoid robot being developed for the US Army to test the special clothing used by soldiers for protection against chemical warfare agents. This bipedal robot weighs about 80kg and is 140(cm) tall at the shoulder. PETMAN, starting from a stand, was able to walk at varying speeds as high as 7.2(km/h). Twenty nine joints, with integrated sensors for measuring position and force, are actuated with either low-fiction hydraulic cylinders, or compact hydraulic rotary actuators [27]. In addition, Boston Dynamics has developed Atlas robot which is based on PETMAN, and has four hydraulically-actuated limbs. It is intended to aid emergency services in search and rescue operations, performing tasks such as shutting off valves, opening doors and operating powered equipment in environments where humans could not survive. Constructed of aluminum and titanium, it stands approximately 1.8 (m) tall, weighs 150(kg). Atlas includes 28 hydraulically actuated degrees of freedom, two hands, arms, legs, feet, and a torso. On February 23, 2016, Boston Dynamics introduced a new version of Atlas which is designed to operate both outdoors and inside buildings. It is specialized for mobile manipulation and is very adept at walking over a wide range of terrain, including snow. This version of Atlas is about 175(cm)tall and weighs 82(kg) [28, 29, 30].

(A) (B)

FIGURE 1.13: Humanoid robot: (a) Petman; and, (b) Atlas.

Currently, there are many small humanoid robots for research and hobby use. For example, we can choose NAO by Aldebaran Robotics [31], DARwIn- OP by ROBOTIS [32], PALRO by FujitSoft [33], or KHR series by Kondo Kagaku Co. Ltd. [34].

Above mentioned researches mainly focused on the locomotion of the robot on flat road, climbing up stairs or walking on slope surface in the indoor environment, except Boston Dynamics. The robots of Boston Dynamics have outstanding performance when moving on rough road in the outdoor environment. However,these robots are both electrically powered and hydraulically actuated. They consumes a lot of energy, meanwhile, for a small robot, it is a big challenge. Thus, my research is focusing on the locomotion of the small robot on rough road considering stability and saving energy.

1.5 Challenges and objective

Achieving movements in human environments is one of the most important goals in humanoid robot research. However, walking on uneven terrains is highly challenging because the robot's feet may have different orientations at every step. In such cases, maintaining the robot's stability is much more difficult than on a flat horizontal terrain. Therefore, related works are relatively less fruitful while abundant researches have been made for walking on even terrains. This research proposed a novel gait generation approach for biped robot on rough road which considers gait generation as an optimization problem with constraints, where constraint function is to ensure the stability of the robot during locomotion.

In addition, in my research, to enhance stability of the robot while walking, I applied toe and arm swing mechanism to protect the robot from the affect of external factors. To be specific, when studying on human foot structure, J. Hughes realize that the toes are in contact for about three-quarters of the walking cycle and exert pressures similar to those from the metatarsal heads. The implication means that the toes play an important part in increasing the weight-bearing area during walking when the heel is raised [35].

Through consideration of current research and development results, I consider some foot structures with toe when investigating locomotion of the robot on flat and rough ground. In toe mechanism, the passive joint using torsion spring is selected as a toe joint. This mechanism is expected to enable the robot to overcome the challenge on uneven terrain by stabilizing walking behavior as depicted in Figure 1.14.

Figure 1.14 describes a working mechanism of robot's toe in motion. During walking, reaction force F_r is exerted by the ground on a foot in contact with it, this force produces an external moment acting on a robot and it makes robot unstable. By adding a toe mechanism using torsion spring, an internal moment M_{lx} is exerted to oppose the external one. Thus, stability of walking behavior is enhanced.

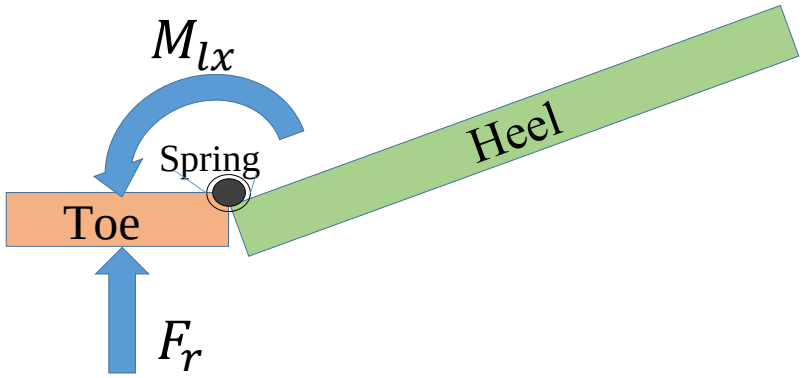

FIGURE 1.14: Reaction moment of toe mechanism.

Besides, on the course of human walking, the leg swing results in an angular momentum that is balanced by the ground reaction moments on the stance foot. Swinging arms create an angular momentum which arises due to the inertial effects of arm swing motion about the vertical axis of the torso in the opposing direction of lower limb rotation, reducing the total angular momentum of the body as shown in Figure 1.15. As can be seen that for moving from pose A to pose B, clockwise moment M_l is required. Simultaneously, the external counter-clockwise moment is also exerted by the ground to counter the motion of leg swing. Meanwhile, because the arms rotate in opposing directions about the lateral axis (axis passing through the shoulders). Thus, the reaction moment from the arms to the trunk precludes ground reaction torque [36]. With mentioned advantage, F. Naoki's research has proposed and modeled physical arm swing model using Adams [37], my research focuses on optimizing this model for walking on rough road.

Finally, I confirmed the success of this approach through the dynamic simulation of the robot walking process by Adams software. In summary, my strategy for achieving the objective of this research is described in Figure 1.16.

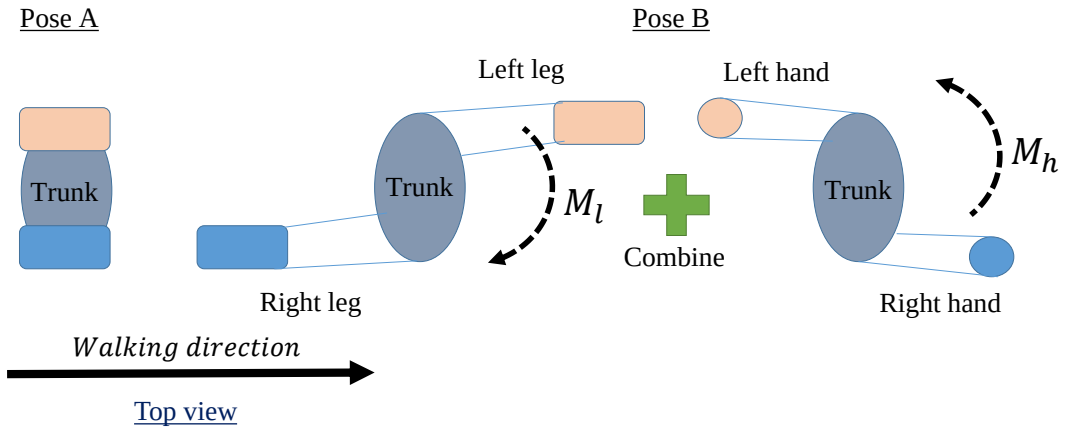

FIGURE 1.15: Arm swing moment opposes to ground reaction moment.

1.6 Simulation Model and Design Tool

1.6.1 Overview of Robot Model

In this research, I used a small biped robot for creating a model for simulation study of walking robot. Currently, a study in the field of robot is widespread and very popular. Therefore, the product of tool kit set was produced in many types such as humanoid robot, biped robot, robot arm, quadruped robot, and hexapod robot. These robots have been produced to meet human requirements both education and entertainment. The small biped robot used in the simulation responds more rapidly and it is popular. As a result, there is a great demand for these devices in the market, but their cost will be reduced every year. Meanwhile, their capabilities and performance are increased. Consequently, I used the small biped robot for making simple simulation models. The model KHR-3HV of Kondo Kagaku Company were used in this study.

The KHR-3HV is the third generation of humanoid robots developed by KONDO KAGAKU Co. Ltd. This is possibly made by up to 22 degrees of freedom with 17 actual servos and 5 dummy servos. The new micro controller board RCB-4 can

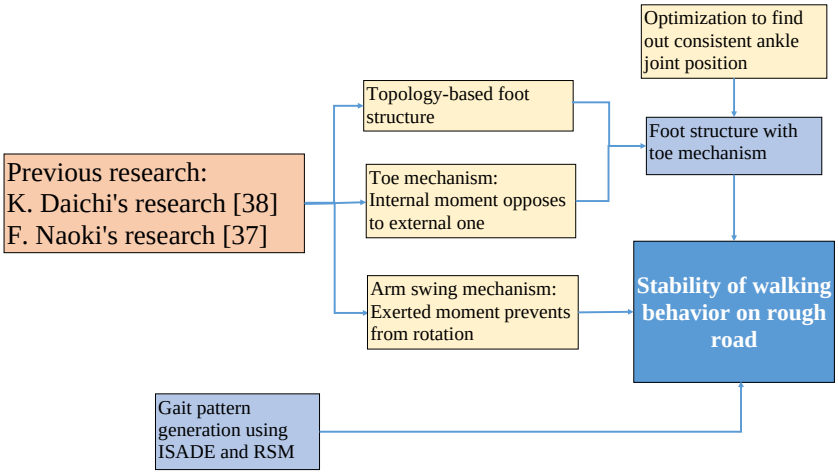

FIGURE 1.16: Strategy for reaching the research's objective.

control up to 35 serial servos. It is compatible with ICS3.0 (serial) servo protocol and a wide range of options parts. The board also includes several extension ports (10xA/D and 10xPIO) which can be applied to a wide range of sensors and extension options [34].

Size	401.05(H) x 194.4(W) mm
Weight	1500 g
Number of servo	17 Digital servo motors
Digital servo motor	KRS-2555HV Servo Specks
	Maximum Operating Angle 270^o
	Maximum Holding Torque 14kgf.cm
	Speed 0.14s/60^o (11.1V, under no load)
	Size 41x21x30.55 mm
	Weight 41.5g
	Operating Voltage 9V 12V

In this paper, the robot KHR-3HV of Kondo Kagaku Company was used to build

a experiment model. Figure 1.17 shows the picture of the real robot and the simulation model whose height is 401mm and weight is 1.5kg, has 10 Degrees of Freedom (DoF) for the legs.

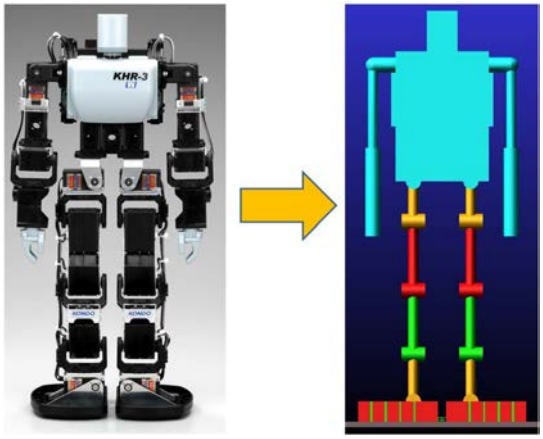

FIGURE 1.17: Real robot and simulation model.

Parameters of model is described as in Figure 1.18 and Table 1.1

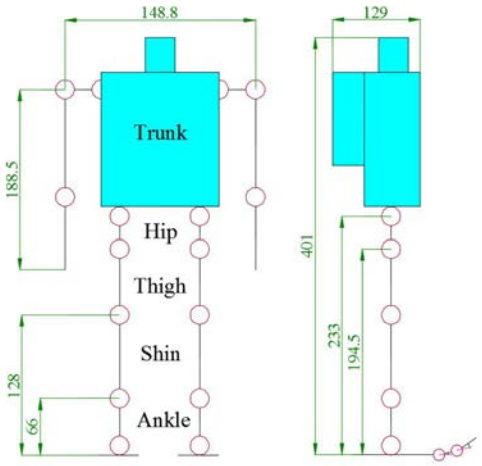

FIGURE 1.18: Robot linkage model.

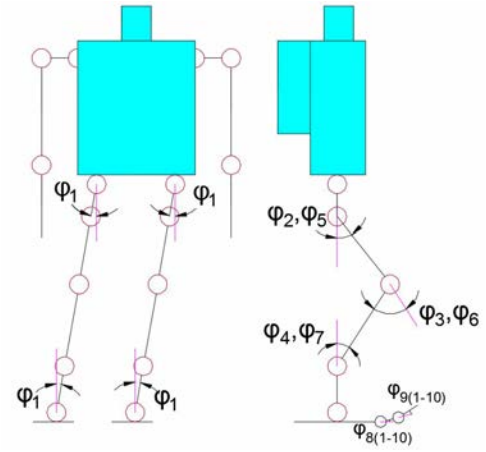

FIGURE 1.19: Definition of joint angles.

The position of joints is defined as described in Figure 1.19. The hip, knee and ankle joints are active joints which are supplied by actuators. Toe joints seldom

TABLE 1.1: Weight of robot's part.

No.	Part	Mass[Gram]
1	Torso	799.4
2	Arm	100
3	Hip	14
4	Thigh	100
5	Shin	65
6	Ankle	37.2
7	Foot	34.1

supplied by using torsion springs, is passive joint. The limited range of joint angles is determined as in Table 1.2.

TABLE 1.2: Definition of joint angles.

Angle	View plane	Leg	Joint	Direction	Value
φ_1	Frontal	Both	Hip and ankle	Side to Side	-15^o to 15^o
φ_2	Sagittal	Right	Hip	Extension and Flexion	-50^o to 50^o
φ_3	Sagittal	Right	Knee	Extension and Flexion	0^o to 60^o
φ_4	Sagittal	Right	Ankle	Extension and Flexion	-50^o to 50^o
φ_5	Sagittal	Left	Hip	Extension and Flexion	-50^o to 50^o
φ_6	Sagittal	Left	Knee	Extension and Flexion	0^o to 60^o
φ_7	Sagittal	Left	Ankle	Extension and Flexion	-50^o to 50^o
$\varphi_{8(1-5)}$	Sagittal	Right	Proximal phalanx	Extension and Flexion	0^o to 30^o
$\varphi_{9(1-5)}$	Sagittal	Right	Distal phalanx	Extension and Flexion	0^o to 30^o
$\varphi_{8(6-10)}$	Sagittal	Left	Proximal phalanx	Extension and Flexion	0^o to 30^o
$\varphi_{9(6-10)}$	Sagittal	Left	Distal phalanx	Extension and Flexion	0^o to 30^o

1.6.2 Adams-MSC software

ADAMS (Automated Dynamic Analysis of Mechanical Systems) is a multi-body dynamics simulation software equipped with Fortran and C++ numerical solvers. ADAMS was originally developed by Mechanical Dynamics Incorporation which then was acquired by MSC Software Corporation. Adams has been proved as very essential to VPD (Virtual Prototype Development) through reducing product time to market and product development costs.

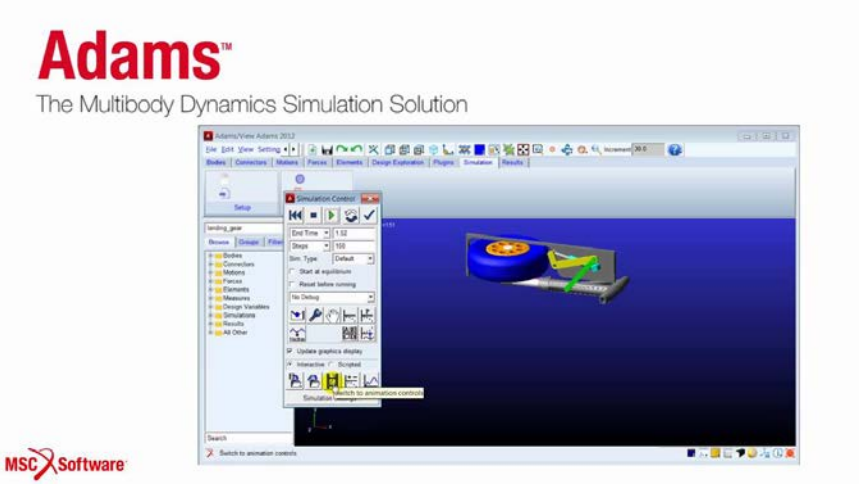

FIGURE 1.20: Adams - MSC software.

Adams helps engineers to study the dynamics of moving parts, and how loads and forces are distributed throughout mechanical systems. Adams improves engineering efficiency and reduces product development costs by enabling early system-level design validation. Engineers can evaluate and manage the complex interactions between disciplines including motion, structures, actuation, and controls to better optimize product designs for performance, safety, and comfort. Along with extensive analysis capabilities, Adams is optimized for large-scale problems, taking advantage of high performance computing environments.

Utilizing multi-body dynamics solution technology, Adams runs nonlinear dynamics in a fraction of the time required by FEA solutions. Loads and forces computed by Adams simulations improve the accuracy of FEA by providing better assessment of how they vary throughout a full range of motion and operating environments.

1.7 Structure of This Dissertation

In order to achieve the aim, a study is implemented by the following steps.

- **First section**: This part presents basic knowledge of robotic field and objective of my research.
- **Second section**: This part describes the approach to generate a gait pattern for the biped robot on flat and rough ground.
- **Third section**: This research investigates the effect of two structure parameters of robot's foot on walking behavior: big toe's width and ankle joint position. Next, the performance of the robot with different toe mechanisms is observed on flat and rough ground.
- **Fourth section**: In this step, I apply a foot structure based on a topology optimization. It enhances the walking capability of the robot on rough road and foot's weight is optimized by removing unnecessary areas. Next is to improve the robot stability by applying an arm swinging mechanism and backbone structure. Finally, I research on an effect of joint characteristic factors on walking performance by Taguchi method.
- **Final section**: This part includes general conclusion of my research and future work.

Bibliography

[1] https://en.wikipedia.org/wiki/Humanoid_robot (Accessed: 20 March 2019).

[2] https://en.wikipedia.org/wiki/Bipedal-gait-cycle (Accessed: 30 May 2016).

[3] http://www.clinicalgaitanalysis.com/history/modern.html (Accessed: 30 May 2016).

[4] J. Perry and J. M. Burnfield, "Gait Analysis: Normal and Pathological Function", 2nd ed., SLACK Incorporated (2010).

[5] M. Vukobratovi ć, and J. Stepanenko, "On the stability of anthropomorphic systems", Mathematical Biosciences (1972), vol. 15, pp. 1–37.

[6] S. Kajita , H. Hirukawa , K. Harada , and K. Yokoi, "Introduction to Humanoid Robotics", Springer Publishing Company, Incorporated (2014).

[7] M. W. Whittle, "An Introduction to Gait Analysis", 4th ed., Oxford (2007).

[8] I. Gonzalez, J. Fontecha, and R. Hervas and J. Bravo, "An Ambulatory System for Gait Monitoring Based on Wireless Sensorized Insoles", Sensor (2015), vol. 15, pp. 16589-16613.

[9] Y. Sakagami, R. Watanabe, C. Aoyama, S. Matsunaga, N. Higaki, and K. Fujimura, "The intelligent ASIMO: System overview and integration", Proceedings of the IEEE/RSJ International Conference on Intelligent Robots and Systems (2002), pp. 2478-2483.

[10] Y. Ogura, H. Aikawa, K. Shimomura, A. Morishima, H.o. Lim, and A. Takanishi, "Development of a new humanoid robot WABIAN-2", Proceedings of IEEE International Conference on Robotics and Automation (2006), pp. 830-835.

[11] Y. Ogura, K. Shimomura, H. Kondo, A. Morishima, T. Okubo, S. Momoki, H.o. Lim, and A. Takanishi, "Human-like Walking with Knee Stretched, Heel-contact and Toe-off Motion by a Humanoid Robot", Proceedings of the International Conference on intelligent robots and systems (2006), pp. 3976-3981.

[12] N. Sugimoto, J. Morimoto, S.-H. Hyon, and M. Kawato, "The eMOSAIC model for humanoid robot control", Neural Netw 29–30 (2012), pp. 8-19.

[13] S. Lohmeier, T. Buschmann, and H. Ulbrich, "Humanoid robot LOLA", Proceedings of IEEE international conference on robotics and automation (2009), pp. 775–780.

[14] B.K. Cho, S.S. Park, and J.H. Oh, "Controllers for running in the humanoid robot, HUBO", Proceedings of IEEE-RAS International Conference on Humanoid Robots (2009), pp. 385–390.

[15] Z. Peng, Y. Fu, Z. Tang, Q. Huang, and T. Xiao, "Online walking pattern generation and system software of humanoid BHR-2", Proceedings of IEEE/RSJ International Conference on Intelligent Robot and Systems (2006), pp. 5471–5476.

[16] G. Metta, G. Sandini, D. Vernon, L. Natale, and F. Nori, "The iCub humanoid robot: an open platform for research in embodied cognition", Proceedings of the 8th Workshop on Performance Metrics for Intelligent Systems (2008), pp. 50–56.

[17] D. Lahr, and D. Hong, "The development of CHARLI: A linear actuated powered full size humanoid robot", Proceedings of the International Conference on Ubiquitous Robots and Ambient Intelligence (2008).

[18] DLR (German Aerospace Center). The robot is complete – arms and hands for TORO, the walking machine,

https://www.dlr.de/dlr/en/desktopdefault.aspx/tabid-10080/150_read-6601/year-2013/150_page-5/#/gallery/9208 (Accessed: 20 March 2019).

[19] C. Ott, C. Baumgärtner, J. Mayr, M. Fuchs, R. Burger, D. Lee, O. Eiberger, A. Albu-Schäffer, M. Grebenstein, and G. Hirzinger, "Development of a biped robot with torque controlled joints", Proceedings of IEEE-RAS International Conference on Humanoid Robots (2010), pp. 167–173.

[20] T. Ishida, "Development of a Small Biped Entertainment Robot QRIO", Proceedings of The Fourth Symposium Micro-Nanomechatronics for Information-Based Society (2004), pp. 23-28.

[21] K. Nishiwaki, S. Kagami, Y. Kuniyoshi, M. Inaba, and H. Inoue, "Toe joints that enhance bipedal and fullbody motion of humanoid robots", Proceedings of IEEE International Conference on Robotics and Automation (2002), pp. 3105-3110.

[22] K. Nishiwaki, S. Kagami, J. J. Kuffner, M. Inaba, and H. Inoue, "Humanoid 'JSK-H7': Research Platform for Autonomous Behavior and Whole Body Motion", Proceedings of the 3rd IARP International Workshop on Humanoid and Human Friendly Robotics (2002), pp. 2-9.

[23] K. Kaneko, F. Kanehiro, S. Kajita, H. Hirukawa, T. Kawasaki, M. Hirata, K. Akachi, and T. Isozumi, "Humanoid robot HRP-2", Proceedings of IEEE International Conference on Robotics and Automation (2004), pp. 1083-1090.

[24] K. Kaneko, K. Harada, F. Kanehiro, G. Miyamori, and K. Akachi, "Humanoid robot HRP-3", Proceedings of IEEE/RSJ International Conference on Intelligent Robots and Systems (2008), pp. 2471-2478.

[25] K. Kaneko, F. Kanehiro, M. Morisawa, K. Akachi, G. Miyamori, A. Hayashi, and N. Kanehira, "Humanoid robot HRP-4 - Humanoid robotics platform with lightweight and slim body", Proceedings of IEEE/RSJ International Conference on Intelligent Robots and Systems (2011), pp. 4400-4407.

[26] S. Kajita, K. Kaneko, F. Kaneiro, K. Harada, M. Morisawa, S. Nakaoka, K. Miura, K. Fujiwara, E. S. Neo, I. Hara, K. Yokoi, and H. Hirukawa, "Cybernetic Human HRP-4C: A humanoid robot with human-like proportions", Robotics Research (2011), pp. 301–314.

[27] G. Nelson, A. Saunders, N. Neville, B. Swilling, J. Bondaryk, D. Billings, C. Lee, R. Playter, and M. Raibert, "PETMAN: A Humanoid Robot for Testing Chemical Protective Clothing", Journal of the Robotics Society of Japan (2012), vol. 30, No. 4, pp. 372-377.

[28] Atlas robot,

https://en.wikipedia.org/wiki/Atlas_(robot) (Accessed: 20 March 2019).

[29] J. Markoff , "Modest Debut of Atlas May Foreshadow Age of 'Robo Sapiens'", New York Times (2013).

[30] T. Hornyak , "Be afraid: DARPA unveils Terminator-like Atlas robot", CNET (2013).

[31] Aldebaran robotics,

http://www.aldebaran-robotics.com (Accessed: 20 March 2019).

[32] ROBOTIS. Open platform humanoid project,

http://www.robotis.com/xe/darwin_en (Accessed: 20 March 2019).

[33] Fujisoft, Inc. PALRO (in japanese),

http://palro.jp/ (Accessed: 20 March 2019).

[34] Products of Kondo Kagaku Co. Ltd. (in Japanese),

http://kondo-robot.com/product /khr-3hv-ver-2-life (Accessed: 30 May 2016).

[35] J. Hughes, P. Clark, L. Klenerman, "The importance of the toes in walking", J Bone Joint Surg Br. (1990), vol. 72, No. 2, pp. 245-251.

[36] J. Park, "Synthesis of natural arm swing motion in human bipedal walking", Journal of Biomechanics (2008), vol. 41, No. 7, pp. 1417-1426.

[37] F. Naoki, "24 時間の連続稼働を目標とした二足歩行ロボットの省エネルギー化" , Masterś thesis (2017), Shibaura Institute of Technology.

[38] K. Daichi, "不整地での歩行安定を目的とした2足歩行ロボット部の最適化" , Masterś thesis (2016), Shibaura Institute of Technology.

Chapter 2

A Gait Generation Method for Biped Robot

Gait generation is very important as it directly effects on the quality of locomotion of biped robots. In point of mathematical view, a gait generation is considered as an optimization problem with constraints, it is readily engaged itself to Evolutionary Computation methods and solutions. This chapter proposes a novel approach based on Response Surface Model and Improve Self-Adaptive Differential Evolution Algorithm (ISADE) for a gait generation problem. This is to aim to enable the robot to walk more naturally and more stably in locomotion.

2.1 Introduction

The first aim of researches carried out in the field of humanoid robot attempts to solve the following problem: How can we build a humanoid prototype able to walk as the humans are doing. This goal is motivated by several applications of the humanoid robot development such assistance, entertainment, medical issues and exploration missions. Hence, they have to move in indoor or outdoor environment and should have the same ability as humans to carry out stable and natural walking.

To reach this target, several works have been done for the generation of the walk of biped robot using the reinforcement learning [1, 2]. Furthermore, a big majority of the walk pattern researches was done based on the zero moment point (ZMP) criterion. Likewise, Kondo et al. [3] described an algorithm for emulations of disabled person's gait based on the ZMP criterion. Also, a constrained analytical trajectory filter [4] was a part of an analytical motion filter using the zero moment point as the stability criteria.

Some works of the walking gaits were based on developing the passive dynamics walking and using other methods such as central pattern generator (CPG) [5]. Also, Narukawa et. al [6] focused on the use of passive dynamics to achieve efficiently walking with simple mechanisms by using a numerical approach.

On the other hand, several researchers consider gait generation as a multiconstrained, multiobjective optimization problem. Gait generation, which combines to control the robot's gait. For instance, human motion captured data has been collected to drive a humanoid robot. However, a number of papers indicate that biological locomotion data can not be used directly for a biped robot caused by kinematic and dynamic discrepancies between humans and the biped robot. This indicates the need for kinematic adjustments in calculating joint angle trajectory [7].

The second strategy considers the gait generation problem of the biped robot as an optimization problem with constraints. The optimal gait cycle is generated by minimizing some performance indexes, for instance, the velocity of motion [8, 9], stability criteria, energy consumption [10, 11, 12, 13], and so on. The gait generation problem of the biped robot often has several objectives and some of which may be inconsistent to each other (for example speed and stability). Hence, it can be said that the gait generation is a multi-constrained and multi-objective optimization problem [14]. These two gait generation strategies may reach the same goal by different methods since both of them actually solve the gait synthesis problem as a multi-constrained multi-objective optimization problem.

Such the goal requires a biped robot that is considerably similar to humans in term of its mechanism and motion pattern, although, the robot with walking ability is astonishing so far. However, it can not be said with certainty that biped robots developed in recent studies realize a "human-like" walk, especially walking on rough road. Therefore, the studies on robot walking is still continuing. This research addresses to an approach to generate a gait pattern for the biped robot. It is an approximated optimization method using RSM and ISADE [15]. In detail, this approach is based on combining two above-mentioned strategies. From human motion captured data, gait functions are interpolated. After that, the optimization problem is formulated to optimize the coefficients of gait function. RSM is applied to define objective and constraint functions.

2.2 System Description

2.2.1 Foot mechanism

During locomotion, the human feet support area continuously varies on the sole of each foot as depicted in Fig. 2.1. The black area is the position where force areas are supported. Wherewith, loading response (LR) is heel only in loading response, mid stance (MSt) is foot flat in mid stance, terminal stance (TSt) is forefoot and toes is terminal stance, and pre-swing (PSw) is medial forefoot in pre-swing. Perry and Burnfield found that the toe contact with ground is quite variable. The onset of toe involvement followed isolated forefoot support by 10% of the stance period. In this period, toe pressures differ markedly with the greatest pressure of the big toe. It ranged between 30% and 55% of that at the heel [16]. Thus, the big toe has an important role in the human walking, especially during the toe-off period.

By this idea, Nerakae and Hasegawa have proposed the foot structure for enhancing the walking behavior of the biped robot [17] as depicted in Fig. 2.2. Their

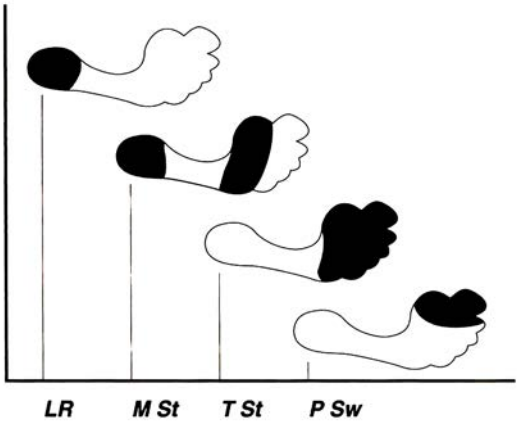

FIGURE 2.1: Sequence of foot support areas during stance [16].

study exhibited that the big toe is a significant part to support and transfer weight from one foot to another foot.

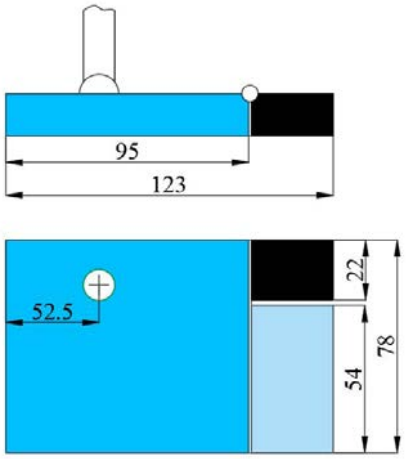

FIGURE 2.2: Robot foot structure.

In toe mechanism, the passive joint using torsion spring was selected as a toe joint. Stiffness coefficient of torsion spring is 1.22$(N.mm/deg)$. Coefficient of friction between foot and the ground is set of 0.5 for heel and 0.17 for toe contact.

2.2.2 Gait generation method

Gait function

Based on the human walking pattern as depicted in Figure 2.3, suppose that the robot control data was generated by the gait function as trigonometric function shown in Eq. 2.1.

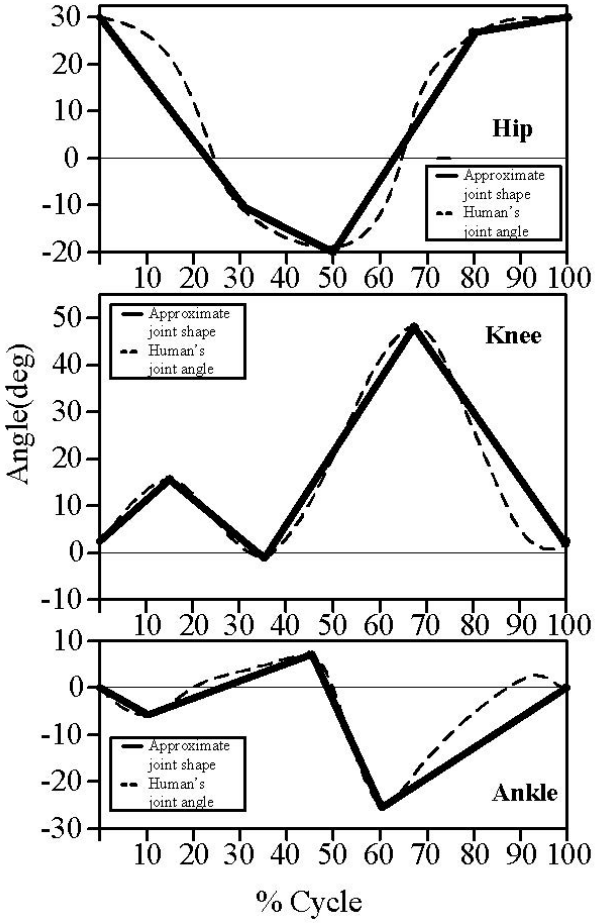

FIGURE 2.3: Waveform of human joint angles in sagittal plane [18, 19].

$$\varphi_i(t) = a_i + b_i cos(\omega t) + c_i sin(\omega t) + d_i cos(2\omega t). \tag{2.1}$$

Where φ_i is angle of i^{th} joint; a_i, b_i, c_i, d_i are coefficients of i^{th} gait function; t is the time, and ω is the angular velocity. By changing *a, b, c, d* coefficients, the gait function will be created to allocate to each joint of the robot.

In this study, the biped robot is considered the locomotion on flat ground with the total time of 4.8s. The robot is simulated in 3 cycles which spend on 3.6s, and 1.2s left is used for checking robot stability. One cycle is set up to 1.2s. As a result, the angular velocity is determined by below simple calculation. In the simulation, one step takes 0.02s, the total number of step is 240. In the second cycle, the biped robot performs its motion the most natural, hence this cycle will be selected to show the waveform of gait function. For walking on rough ground, the locomotion of the robot is considered in 7.2s including 5 cycles (6s) and 1.2s for checking stability.

$$\omega = \frac{2\pi}{1.2} = 5.236$$

Gait pattern on flat ground The gait functions which are assigned to all joints are described by Eq. 2.2 - Eq. 2.8.

$$\varphi_1 = \begin{cases} 0; & t = 0 \; or \; t \geq 3.6 \\ \pm 1.5; & t = 0.3 \; \& \; t = 3.3 \\ \varphi_1(t); & 0.3 < t < 3.3 \end{cases} \quad (2.2)$$

$$\varphi_3 = \begin{cases} 0; & t \leq 0.3 \; or \; t \geq 3.6 \\ \varphi_3(t + 0.6); & 0.3 < t < 3.3 \\ 30; & t = 3.3 \end{cases} \quad (2.4)$$

$$\varphi_2 = \begin{cases} 0; & t \leq 0.3 \; or \; t \geq 3.6 \\ \varphi_2(t + 0.6); & 0.3 < t < 3.3 \\ 15; & t = 3.3 \end{cases} \quad (2.3)$$

$$\varphi_4 = \begin{cases} 0; & t \leq 0.3 \; or \; t \geq 3.6 \\ \varphi_4(t + 0.6); & 0.3 < t < 3.3 \\ 15; & t = 3.3 \end{cases} \quad (2.5)$$

$$\varphi_5 = \begin{cases} 0; & t = 0 \; or \; t \geq 3.3 \\ 15; & t = 0.3 \\ \varphi_2(t); & 0.3 < t < 3.3 \end{cases} \quad (2.6) \qquad \varphi_7 = \begin{cases} 0; & t = 0 \; or \; t \geq 3.3 \\ 15; & t = 0.3 \\ \varphi_4(t); & 0.3 < t < 3.3 \end{cases} \quad (2.8)$$

$$\varphi_6 = \begin{cases} 0; & t = 0 \; or \; t \geq 3.3 \\ 30; & t = 0.3 \\ \varphi_3(t); & 0.3 < t < 3.3 \end{cases} \quad (2.7)$$

Gait pattern on rough ground The gait functions which are assigned to all joints are described by Eq. 2.9 - Eq. 2.15.

$$\varphi_1 = \begin{cases} 0; & t = 0 \; or \; t \geq 6.0 \\ \pm 1.5; & t = 0.3 \; \& \; t = 5.7 \\ \varphi_1(t); & 0.3 < t < 5.7 \end{cases} \quad (2.9) \qquad \varphi_4 = \begin{cases} 0; & t \leq 0.3 \; or \; t \geq 6.0 \\ \varphi_4(t + 0.6); & 0.3 < t < 5.7 \\ 15; & t = 5.7 \end{cases} \quad (2.12)$$

$$\varphi_2 = \begin{cases} 0; & t \leq 0.3 \; or \; t \geq 6.0 \\ \varphi_2(t + 0.6); & 0.3 < t < 5.7 \\ 15; & t = 5.7 \end{cases} \quad (2.10) \qquad \varphi_5 = \begin{cases} 0; & t = 0 \; or \; t \geq 5.7 \\ 15; & t = 0.3 \\ \varphi_2(t); & 0.3 < t < 5.7 \end{cases} \quad (2.13)$$

$$\varphi_3 = \begin{cases} 0; & t \leq 0.3 \; or \; t \geq 6.0 \\ \varphi_3(t + 0.6); & 0.3 < t < 5.7 \\ 30; & t = 5.7 \end{cases} \quad (2.11) \qquad \varphi_6 = \begin{cases} 0; & t = 0 \; or \; t \geq 5.7 \\ 30; & t = 0.3 \\ \varphi_3(t); & 0.3 < t < 5.7 \end{cases} \quad (2.14)$$

$$\varphi_7 = \begin{cases} 0; & t = 0 \; or \; t \geq 5.7 \\ 15; & t = 0.3 \\ \varphi_4(t); & 0.3 < t < 5.7 \end{cases} \tag{2.15}$$

In the toe mechanism, since the energy consumption reduction of the robot is considered, the passive joint is selected as a toe joint. Consequently, φ_{8r} and φ_{8l} are restricted in (0^o-30^o) range. Their values depend on the robot's geometric posture and the impact forces in its walking process.

Problem formulation

The concept of the optimization process is shown as in Figure 2.4. Z_f and X_f denote the distance from the initial position to final position along z-axis and x-axis in the robot locomotion, respectively. R_f is the angle of rotation.

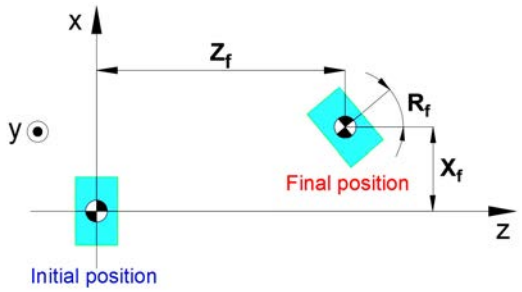

FIGURE 2.4: Overview of optimization.

Definition of optimal design is described as Eq. 2.16 - Eq. 2.23.

The design variables (DVs) are

$$x = [a_i, b_i, c_i, d_i], \; i = 1 \div 4. \tag{2.16}$$

Where a_i, b_i, c_i, d_i (i=1, 2, 3, 4) are the coefficients of the gait function. Range of design variables is predefined as in Table 2.1.

TABLE 2.1: Range for design variables.

Design variables	Lower boundary	Upper boundary
a_1	0	0.006
b_1	0	0.1
c_1	0	0.002
d_1	-0.01	0
a_2	0	0.08
b_2	0	0.4
c_2	0	0.001
d_2	0	0.02
a_3	0	0.8
b_3	0	0.08
c_3	-0.4	0
d_3	-0.2	0
a_4	-0.4	0
b_4	0	0.3
c_4	0	0.2
d_4	0	0.1

The constraint functions are

$$g_1(x) = 20 - |X_f| \geq 0. \qquad (2.17)$$

$$h_1(x) = 243.53 - Y_f = 0. \qquad (2.19)$$

$$g_2(x) = 5 - |R_f| \geq 0. \qquad (2.18)$$

$$h_2(x) = N - 240 = 0. \qquad (2.20)$$

To find out design variables, it should have 4 constraint functions. In which, the restrictions of X_f distance and R_f angle as shown in Eq. 2.17, Eq. 2.18 guarantee that the biped robot can walk straight and stably. In Eq. 2.19, Y_f is the distance from the center of mass (CoM) to the ground along y axis, Y_f must be equal to 243.53mm to ensure the robot not to slip and fall at the final framework. However, in simulation, Y_f at beginning position always differs from it at final position (It is changed a little bit by about 10^{-2} to 10^{-1} due to calculation error). Thus, I set 243mm < Y_f <244mm in optimization. In Eq. 2.20, N is the number of simulation step. N is equal to 240 for flat ground (360 for rough ground) to check the success of the simulation. I

realize that if Eq. 2.19 is satisfied, Eq. 2.20 is also achieved, so, I don't use Eq. 2.20 in optimization but setting it in simulation. Equation 2.17 - 2.20 will be also checked again when the simulation finishes.

The objectice function is

$$f(x) = -Z_f \rightarrow min. \tag{2.21}$$

The penalty function is

$$p(x) = \Sigma_{i=1}^{2} min[g_i(x), 0]^2 + [h_1(x)]^2. \tag{2.22}$$

The modified objective function is

$$F(x) = -Z_f + \gamma.p(x) \rightarrow min. \tag{2.23}$$

Where γ is a penalty coefficient set to 1000.

Improved self-adaptive differential evolution

Differential evolution (DE) is an optimization technique originally proposed by Storn and Price [20]. It is categorized into evolution algorithm group, which is characterized by operators of mutation and crossover. In DE, two important coefficients, which play key roles to decide the correction and speed of convergence, are scaling factor F and crossover rate Cr. Another important parameter in DE, population size NP remains a user-assigned value to cope with problem complexity. ISADE not only adaptively changes those three coefficients but also integrate different mutation schemes to take advantages of them.

Adaptive learning strategies selection In [15], Tam Bui et al. randomly chose three mutation schemes, which are *DE/best/1/bin*, *DE/best/2/bin*, and *DE/rand best/1/bin*.

Among DE's schemes, *DE/best/1/bin* and *DE/best/2/bin* are known for good convergence property and *DE/rand best/1/bin* is known for good diversity. The probability of applying those strategies are equally assigned at with values p_1 = p_2 = p_3 = *1/3*. Equation 2.24 - Equation 2.26 show the formula of chosen schemes.

$$\text{DE/best/1: } V_{i,j}^G = X_{best,j}^G + F * (X_{r_1,j}^G - X_{r_2,j}^G) \tag{2.24}$$

$$\text{DE/best/2: } V_{i,j}^G = X_{best,j}^G + F * (X_{r_1,j}^G - X_{r_2,j}^G) + F * (X_{r_3,j}^G - X_{r_4,j}^G) \tag{2.25}$$

$$\text{DE/rand to best/1: } V_{i,j}^G = X_{r_1,j}^G + F * (X_{best,j} - X_{r_1,j}^G) + F * (X_{r_2,j}^G - X_{r_3,j}^G) \tag{2.26}$$

where r_1, r_2, r_3, r_4, and r_5 are randomly selected integers in the range [1, NP], where NP is the population size.

In APGA/VNC approach proposed by Tooyama and Hasegawa [21] scaling factor changes according to iteration as sigmoid function as in Eq. 2.27.

$$F_i = \frac{1}{1 + exp\left(\alpha * \frac{i - \frac{NP}{2}}{NP}\right)} \tag{2.27}$$

where α, i denote the gain of the sigmoid function, particle of i^{th} in NP, respectively.

ISADE adds a new factor to calculate F as shown in Eq. 2.28.

$$F_{iter}^i = \frac{F_i + F_{iter}^{mean}}{2} \tag{2.28}$$

where $iter = 1, \ldots, iter_{max}$, $i = 1, \ldots, NP$ and F_{iter}^{mean} is calculated as Eq. 2.29.

$$F_{iter}^{mean} = F_{min} + (F_{max} - Fmin)\left(\frac{iter_{max} - iter}{iter_{max}}\right)^{n_{iter}} \tag{2.29}$$

where F_{max}, F_{min} denote the lower and upper boundary condition of F with recommended values of 1.55 and 0.15, respectively. $iter$, $iter_{max}$ and n_{iter} denote the current, maximum generation, and nonlinear modulation index as Eq. 2.30.

$$n_{iter} = n_{min} + (n_{max} - n_{min})\left(\frac{iter}{iter_{max}}\right) \tag{2.30}$$

where n_{max} and n_{min} are typically chosen in the range $(0, 15]$. Recommended values for n_{min} and n_{max} are 0.2 and 6.0, respectively.

Adaptive learning strategies selection ISADE algorithm is able to detect whether high values of C_r are useful and if a rotationally invariant crossover is required. A minimum base for C_r around its median value is incorporated to avoid stagnation around a single value. The control parameter C_r is assigned as Eq. 2.31.

$$C_r^{i+1} = \begin{cases} rand_2 & \text{if } rand_1 \leq \tau \\ C_r^i & \text{otherwise.} \end{cases} \tag{2.31}$$

where: $rand_1$ and $rand_2$ are uniform random values $\in [0, 1]$, τ represents probabilities to adjust C_r, which is updated using Eq. 2.32.

$$C_r^{i+1} = \begin{cases} C_{r_{min}} & \text{if } C_{r_{min}} \leq C_r^{i+1} \leq C_{r_{medium}} \\ C_{r_{max}} & \text{if } C_{r_{medium}} \leq C_r^{i+1} \leq C_{r_{max}} \ . \end{cases} \tag{2.32}$$

where: $C_{r_{min}}$, $C_{r_{medium}}$ and $C_{r_{max}}$ denote the low value, median value and high value of crossover parameter, respectively. As recommended in [15], this research takes $\tau = 0.10$, $C_{r_{min}} = 0.05$, $C_{r_{medium}} = 0.50$ and $C_{r_{max}} = 0.95$.

Response Surface Model

Generating a gait pattern for the biped robot using RSM and evolutionary algorithms (EAs) was applied by Ito and Hasegawa [18] at the first time, Nerakae and Hasegawa [22] after. The gait generation method presented by the later work performs the more powerful approach in comparison with Simulated Annealing (SA) algorithm in the former. However, above-mentioned works were unsuccessful when considering locomotion of the robot on rough road. Our paper introduces one more approach which applies Improved Self-Adaptive Differential Evolution (ISADE) algorithm [15] and Response Surface Model (RSM) to generate a gait pattern for Kondo KHR-3HV robot while walking on flat and rough road. ISADE has been confirmed to improve the calculation cost, and the stability of convergence towards the optimal solution has a good performance while solving the multi peak optimization problems with multi dimensions. RSM of 3^{rd} order is used to approximate the response of the simulation. The 3^{rd} order model is described by a polynomial function as Eq. 2.33:

$$\tilde{P}(x) = a_{po} + \Sigma_{i=1}^{n} b_{pi} x_i + \Sigma_{i=1}^{n} c_{pii} x_{ii}^2 + \Sigma_{ij(i<j)} c_{pij} x_i x_j + \Sigma_{i=1}^{n} d_{pii} x_{ii}^3. \tag{2.33}$$

Where n is a number of variable, x_{pi} is a set of inputs, and a_p, b_p, c_p, d_p are the polynomial coefficients. The number of sampling for initialization equaled to the number of the polynomial coefficients is calculated by Eq. 2.34.

$$N_s = \frac{(n+1)(n+2)}{2} + n. \tag{2.34}$$

Where n should be 16. Thus, the number of samples must be 169 for the calculation of all polynomial coefficients. The approximated optimization process is depicted as Fig. 2.5.

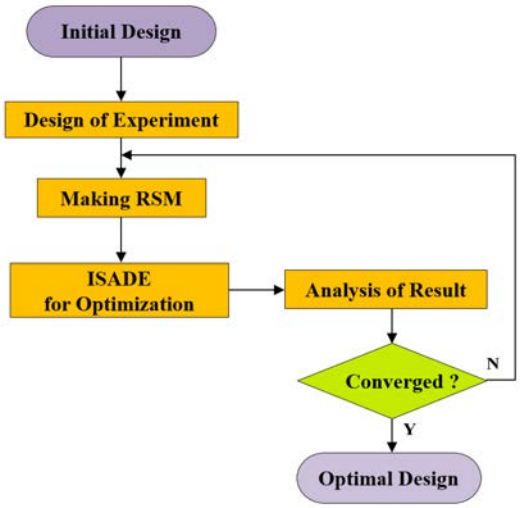

FIGURE 2.5: Overview of optimization process.

Combination of ISADE and RSM

- Initial design is initialized by specifying the simple analysis.
- Samples are simulated in Adams environment.
- Making the RSM
- The design variables are optimized by ISADE algorithm based on RSM.
- The design variables from step 4 are used to check constraint functions again through the simulation.
- The convergence is checked. If this is achieved, the optimal process will be terminated. Oppositely, the repetition will begin from step 3.

2.2.3 Environment

Surfaces shown in Fig. 2.5 is used to perform locomotion of the robot. The first type is perfectly flat ground. The second one is 4mm-high wave rough road consisting of a positive and a negative wave such as normal surface in indoor and outdoor environment in reality.

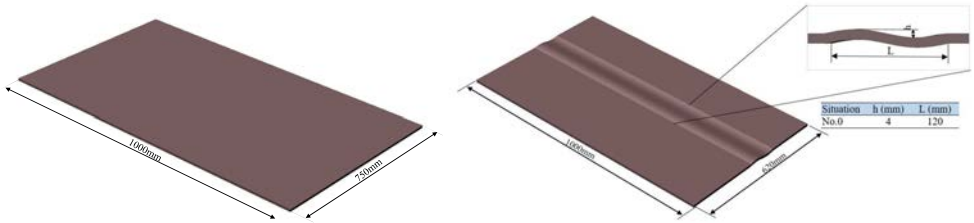

(A) (B)

FIGURE 2.6: Environment: (a) Flat ground; and (b) 4mm-high wave ground.

2.2.4 Simulation result

The optimal value for the design variable is presented in Table 2.2. By returning these coefficients to the gait function described in Eq. 2.1. Four gait functions will be generated to assign to all of joint of the robot, which follows the principle as shown by Eq. 2.2 - Eq. 2.8.

TABLE 2.2: Value for design variables.

i	Design variables for flat ground			
	a_i	b_i	c_i	d_i
1	0.003	0.021	0.001	-0.006
2	0.034	0.231	0.001	0.013
3	0.395	0.037	-0.233	-0.162
4	-0.218	0.165	0.149	0.075
i	Design variables for rough ground			
1	0.003	0.054	0.001	-0.008
2	0.032	0.180	0.001	0.011
3	0.427	0.039	-0.147	-0.144
4	-0.232	0.111	0.102	0.073

The waveform of control data for both of situations are depicted in Fig. 2.7. Result of simulation is shown in Fig. 2.8. As can be seen that the robot can walk normally on flat ground and overcome 4mm-high obstacle on rough terrain.

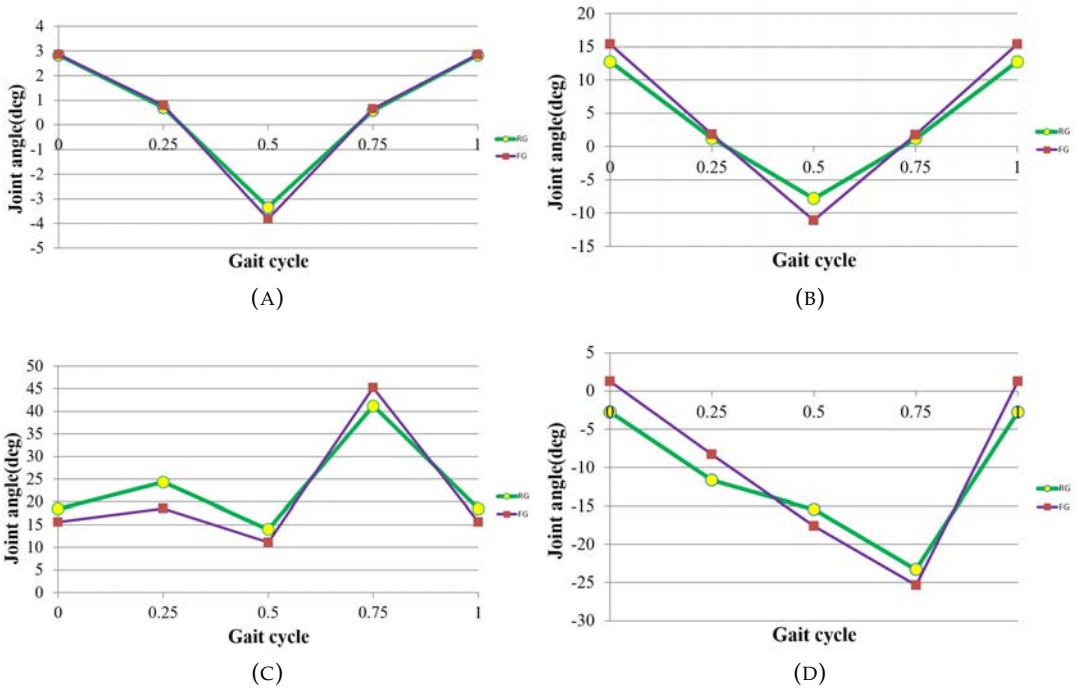

FIGURE 2.7: Waveform of the gait function: (a) Hip and ankle roll joint angle; (b) Hip pitch joint angle; (c) Knee pitch joint angle; and, (d) Ankle pitch joint angle.

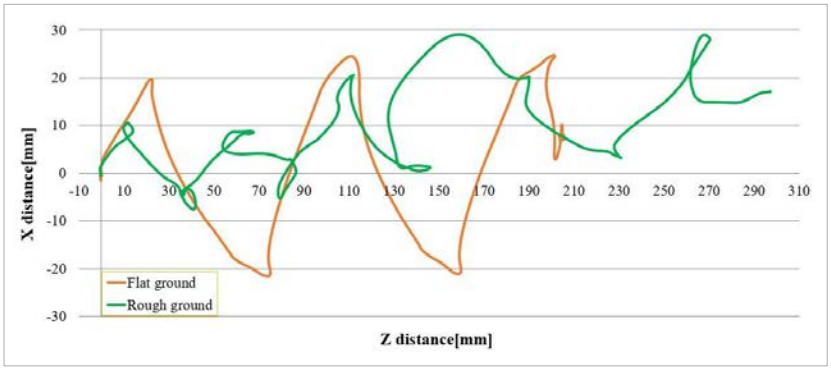

Situation	Walking distance (mm)	Lateral distance (mm)	Angle of rotation (º)
Flat ground	203.83	7.43	-5.10
Rough ground	297.55	15.77	-2.95

FIGURE 2.8: Simulation result.

A consideration of the gait similarity between the robot and the human in locomotion on flat ground is depicted as in Figure 2.9. The robot gait at time 1.2s likes an "Initial contact period" of the human gait, at time 1.5s likes "Midstance period", at time 1.8s likes "Terminal stance period", at time 2.1s likes "Initial swing period" where it can be observed the bending of toes and at time 2.4s likes "Terminal swing period". The differences of posture are expected to occur as a consequence of the physical structure dissimilarity with the human's structure. The waveform of gait function allocated to all joints of the robot is shown in Figure 2.7. As can be seen, the wave forms of hip and knee joint gait function are similar to that of human beings.

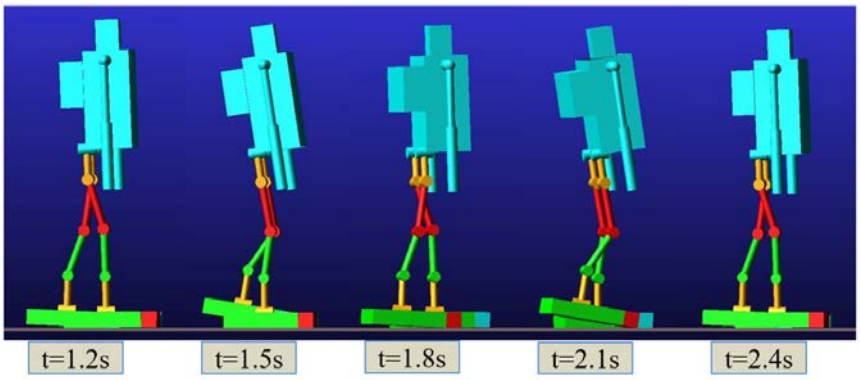

FIGURE 2.9: Gait behavior of the biped robot in a cycle.

2.3 Conclusion

A gait pattern generation is a very challenging task in the biped robot area. Recently, the approach of using EAs, especially new methods, proved their potential of tackling gait generation problem based on their effectiveness on searching for optimal result. In this section, to generate walking gait of a small biped robot, a novel gait pattern generation method is proposed based on ISADE and RSM. Through the dynamic simulation of the robot in Adam environment, the result showed that this

approach successfully produces gait pattern for KHR-3HV biped robot during locomotion on flat and 4mm-high wave ground.

Bibliography

[1] L. Yang, C. M. Chew, Y. Zheng, and A. N. Poo, "Truncated Fourier series formulation for bipedal walking balance control," Robotica (2010), vol. 28, pp. 81-96.

[2] T. Li, Y. T. Su, S. W. Lai, and J. J. Hu, "Walking motion generation, synthesis, and control for biped robot by using PGRL, LPI, and fuzzy logic," IEEE trans. On Systems, Man, and Cybernetics, Part B: Cybernetics (2011), vol. 41, pp. 736-748.

[3] H. Kondo, Y. Ogura, H. Aikawa, A. Morishima, J. Shimizu, H. Lim, and A. Takanishi, "Application of biped humanoid robot to simulate the motion of elderly and disable people," Gerontechnology, vol. 7, p. 143.

[4] K. Muecke and D. Hong, "Constrained analytical trajectory filter for stabilizing humanoid robot motions," Intelligent Service Robotics (2011), vol. 4, pp. 203-218.

[5] C. Fu, F. Tan, K. Chen, "A simple walking strategy for biped walking based on an intermittent sinusoidal oscillator," Robotica (2010), vol. 28, pp. 869-884.

[6] T. Narukawa, M. Takahashi, and K. Yoshida, "Efficient walking with optimization for a planar biped walker with torso by hip actuators and springs," Robotica (2011), vol. 29, pp. 641-648.

[7] C. Zhou, P. K. Yue, J. Ni, and S. B. Chan, "Dynamically stable gait planning for a humanoid robot to climb sloping surface," Proc. Of IEEE Int. Conf. on Robotics, Automation and Mechatronics (2004), pp. 341-346.

[8] M. Aghaabbasloo, M. Azarkaman, and M. E. Salehi, "Biped robot joint trajectory generation using PSO evolutionary algorithm," 3rd Joint Conf. of Al & Robotic and 5th RoboCup Iran Open Int. Symp. (2013), pp. 1-6.

[9] P.H. Kuo, Y.F. Ho, K.F. Lee, L.H. Tai, and T.H.S. Li, "Development of Humanoid Robot Simulator for Gait Learning by Using Particle Swarm Optimization", Proceedings of the IEEE International Conference on Systems, Man and Cybernetics (2014), pp. 2684-2688.

[10] Z. Tang, Z. Sun, and C. Zhou, "GA Based Optimization for Humanoid Walking", ICGST- ARAS Journal (2006), vol. 5, pp. 1-10.

[11] B.H. Lee, J.S. Kong, and J.G. Kim, "Optimal Trajectory Generation for a Humanoid Robot Based on Fuzzy and Genetic Algorithm", IEEE Congress on evolutionary computation (2006), pp. 1968-1974.

[12] T. Arakawa and T. Fukuda, "Natual motion trajectory generation of biped locomotion robot using genetic algorithm through energy optimization," Proc. Of IEEE Int. Conf. on Systems, Man, and Cybernetics (1996), vol. 2, pp. 1495-1500.

[13] L. Hu, C. Zhou, and Z. Sun, "Estimating biped gait using spline-based probability distribution function with Q-learning," IEEE Trans. On Industrial Electronics, vol. 55, pp. 1444-1452, 2008.

[14] K. Seo and S. Hyun, "Genetic programming based automatic gait generation for quadruped robots," Proc. Of the 10th Annual Genetic and Evolutionary Computation Conference (2008), pp. 293-294.

[15] T. Bui, H. Pham, and H. Hasegawa, "Improve self-adaptive control parameters in differential evolution for solving constrained engineering optimization problems", Journal of Computational Science and Technology (2013), no. 1, vol. 7, pp. 59-74.

[16] J. Perry and J. M. Burnfield, "Gait Analysis: Normal and Pathological Function", 2nd ed., SLACK Incorporated (2010).

[17] K. Nerakae and H. Hasegawa, "Big toe sizing design of small biped robot by using gait generation method", Applied Mechanics and Materials (2014), vol. 541-542, pp. 1079-1086.

[18] N. Ito and H. Hasegawa, "The Robust Design to Generate the Gait Pattern of a Small Biped Robot", Japan Society for Design Engineering (2010), no. 6, vol. 45, pp. 48-55.

[19] M. W. Whittle, "An Introduction to Gait Analysis", 4th ed., Oxford (2007).

[20] R. Storn and K. Price, "Differential Evolution-A simple and efficient heuristic for global optimization over continuous spaces", Journal Global Optimization (1997), vol. 11, pp. 341-359.

[21] S. Tooyama and H. Hasegawa, "Adaptive Plan System with Genetic Algorithm using the Variable Neighborhood Range Control", Proceedings of IEEE Congress on Evolutionary Computation (2009), pp. 846-853.

[22] K. Nerakae and H. Hasegawa, "Simulation Based Design Optimization Framework for a Gait Pattern Generation of a Small Biped Robot with Tiptoe mechanism", Proceedings of the 10th International Conference on Modeling and Applied Simulation (2014), pp. 295-302.

Chapter 3

Effect of Structure Parameter on Biped Walking Behavior

This chapter addresses the effect of two structure parameters on the walking behavior of a biped robot. The applied foot structure consists of a tiptoe and a big toe inspired by the human foot which has a crucial role in moving stability. The gait generation method finding the proper position of ankle joint is applied by varying the ankle joint position. There are two requirements in the robot motion: go straight and stay within setting conditions. This chapter is implemented in three stages. Firstly, the effect of big toe's size on the biped walking behavior is considered. In the second stage, the simulations of all the robot models which have the different ankle joint position are implemented. The results are compared to the human ankle joint trajectory in gait performance to observe the effect of ankle joint position on the walking behavior. Finally, some foot structures with toe mechanisms are investigated on flat and ground road.

3.1 Introduction

The human body has a complicated physical structure and implements difficult movements. During the past several decades, many researchers have concentrated

on the field of the biped robot inspired by the human body [1, 2, 3, 4]. The first aim of researches carried out in this field attempts to solve the following problem: "How can the robot walk naturally and stably ?". This goal is motivated by several applications of the biped robot development such assistance, entertainment and medical issues. Hence, they have to move in a domestic environment and should have the same ability as the humans to carry out stable walking.

In most previous studies, the feet of the biped robot have been designed with the rigid flat sole structure which can not provide the best contact with the ground while in locomotion. Sometimes, it is a point contact at the corner of the sole as depicted in Fig. 3.1, thus, the number of the contact point reduces. Consequently, the support polygon area and the stability of the robot also decrease.

Furthermore, one of the characteristics of the human walk is heel-contact and toe-off motion in steady walking. Implementing adaptive walking, a foot is one of the most important regions of the human body in bipedal locomotion because it is the only region that has a direct physical interaction with the environment. The human foot has a complicated structure which consists of toes and several joints. On the human walking cycle, this structure makes the ground reaction force smoothly change in toe-off. Thus, it helps the contact between the human foot and the ground be smooth, has an important role in walking stability.

Overcoming this challenge, being inspired by the human foot, there have been some papers mentioned on the flexible foot structure for the biped robot. For instance, Yu Ogura et al. have proposed a new foot mechanism by implementing one passive joint for bending toe motion of Wabian-2R. However, in this study, the number of the robot's Degree of Freedom (DoF) is reduced due to the predetermination is complemented by waist rolling motion [5]. Yamane and Trutoiu has investigated feet composed of curved surfaces at toe and heel and also a flat section for a simple planar biped robot [6]. Sellaouti et al. has developed the new model of the humanoid robot HRP-2 with passive tiptoe joints to enhance its walking speed [7].

In [8], the humanoid robot LOLA with an actively driven toe joints has been designed by Lohmeier et al. However, the papers mentioned above mainly focus on the humanoid robot whose parameters are similar to the human ones. The human-size robots are convenient for designing structure and integrating an actuator on the feet.

By the contrary, a small robot has difficulty in building a foot structure by limited parameters. In this area, Nerakae and Hasegawa has presented the foot mechanism with a big toe and a tiptoe for the 10 DoF small biped robot [9]. In motion, to perform walking behavior like humans, rigid flat sole structure is inappropriate because it can touch the ground by point or line contact in toe-off period as depicted in Fig. 3.1. Meanwhile, foot structure proposed by Nerakae and Hasegawa equips the robot with a better contact: Plane contact. It enables the foot to increase the contact points and improves the stability as described in Fig. 3.2. Nevertheless, in their research, the trajectories of all the joints on both legs are generated by seven isolated gait functions which makes a gait pattern generation problem be complicated. Also, the ankle joint position based on the reference of the real robot is fixed. In my point of view, I consider that ankle joint position has the big effect on the walking behavior as well as the gait pattern of the biped robot. Thus, when building the novel foot structure, the ankle joint position needs to be changed.

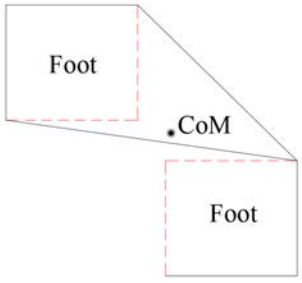

FIGURE 3.1: An example presenting the contact points, the support polygon and its center of mass (CoM).

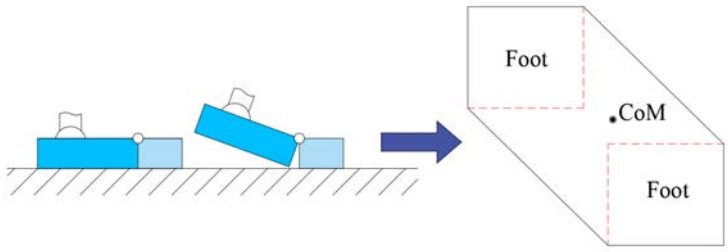

FIGURE 3.2: An foot structure with toes.

3.2 Contributions

This study continues to develop the foot structure for the small biped robot proposed by Nerakae and Hasegawa [9]. The paper implements to investigate the effect of two parameters: big toe's size and ankle joint position on the robot walking behavior. The investigation is to aim to determine the consistent big toe's size for the toe mechanism when the robot performs its locomotion on the flat ground. In the next stage, this paper considers the effect of the ankle joint position on the robot walking behavior and gait functions. The simulation results of all the biped robot models are compared with the human walking behavior.

3.3 Foot Structure

To continue studying on a foot structure proposed by Nerakae as described in Figure 3.3, our work is based on the assumption that this parameter has an effect on the walking behavior and distance, gait function. It is considered in a predefined range as described in Table 3.1, and Table 3.2. In the first simulation, the ankle joint position is based on the real robot with p = 52.5mm and control data are collected from Figure 2.7 in Part II. In second simulation, gait pattern is generated by applying ISADE and RSM.

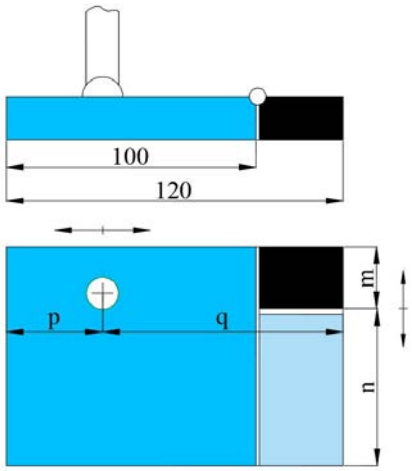

FIGURE 3.3: Robot foot structure.

TABLE 3.1: Big toe's size detail.

No.	m[mm]	n[mm]	Ratio= m/(m + n)
F1	20	58	0.26
F2	22	56	0.28
F3	24	54	0.31
F4	26	52	0.33
F5	28	50	0.36
F6	30	48	0.38
F7	32	46	0.41
F8	34	44	0.44
F9	36	42	0.46
F10	38	40	0.49

TABLE 3.2: Ankle joint position.

No.	p[mm]	q[mm]	Ratio= p/(p + q)
N1	80	40	0.67
N2	70	50	0.58
N3	60	60	0.50
N4	50	70	0.42
N5	40	80	0.33
N6	30	90	0.25
N7	20	100	0.17

3.4 Simulation results

First simulation. The control data of this simulation is shown in Figure 2.7. As has been pointed out in Table 3.3 and Fig. 3.4 that the robot walking distances are almost same between all the models, the side distance and the angle of rotation have a small change in value. It can be said that with the new gait generation approach, the big toe's width has no significant effect on the robot walking behavior. This study selected F2 structure along with the ratio of 0.28 for doing the second simulation.

TABLE 3.3: Simulation result of experiment I.

No.	Walking distance (mm)	Lateral distance (mm)	Angle of rotation (^{o})
F1	204	7.72	4.89
F2	204	7.43	5.10
F3	203	8.02	4.75
F4	203	4.16	6.14
F5	202	6.53	4.65
F6	202	6.54	3.27
F7	204	9.68	2.27
F8	204	6.68	3.45
F9	201	5.96	3.41
F10	200	6.03	1.57

Second simulation. The result of the second simulation is shown in Fig. 3.5. The robot ankle joint trajectory of all the experiments is shown in Fig. 3.6a, this data is collected in the second cycle since the biped robot performs the most natural and stable locomotion. By comparison, the human ankle joint trajectory is depicted in Fig. 3.6b, the subject in this experiment was a man. He was 33 years old, 164 cm in height, and weighed 49.5 kg. The kinematic data for the lower body while walking was captured by a motion capture system. Data was recorded at a sampling rate of 200 Hz while the subject was walking.

As can be seen, in general, the robot ankle joint trajectory has a frequency and a trend similar to the human one. From N1 to N7, the height of the ankle joint

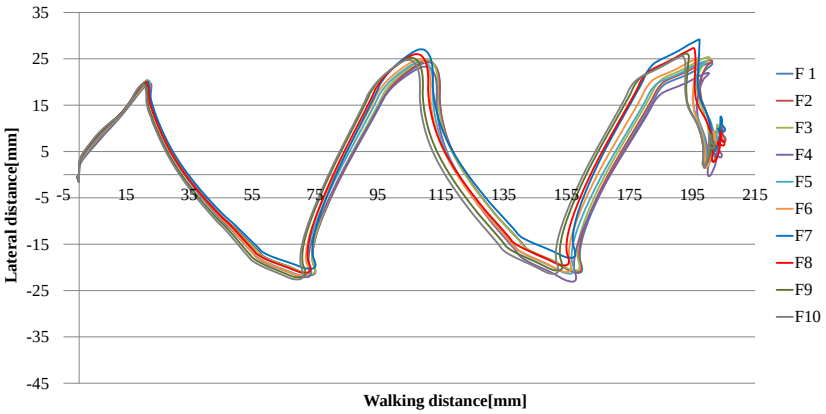

(A)

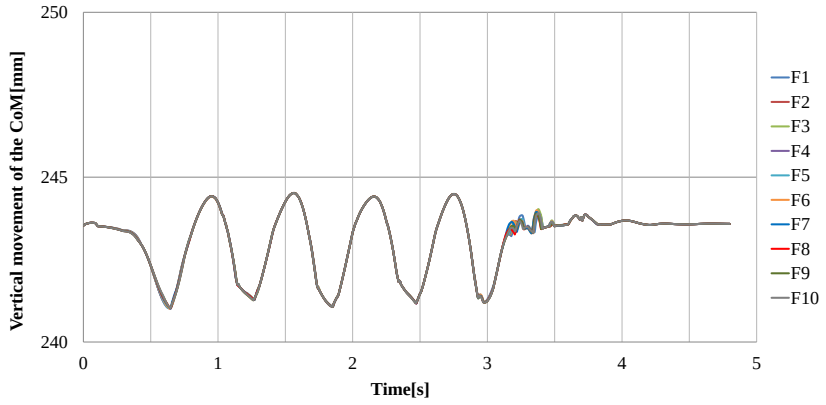

(B)

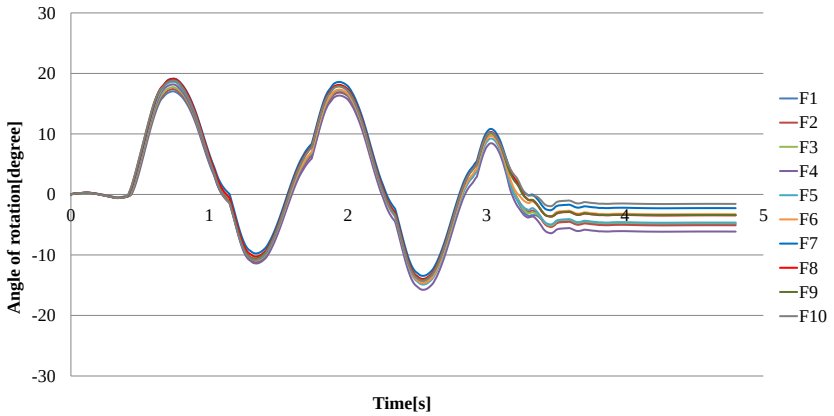

(C)

FIGURE 3.4: Simulation result: (a) CoM trajectory on flat ground; (b) Vertical movement of the CoM; and (c) Angle of rotation.

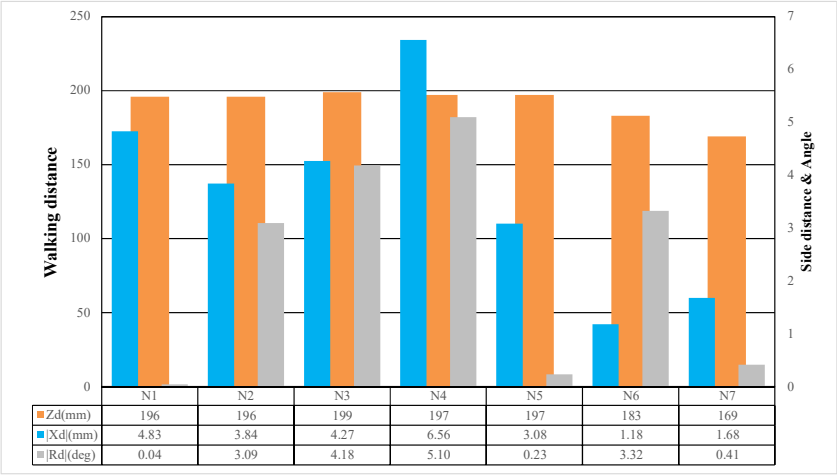

	N1	N2	N3	N4	N5	N6	N7
Zd(mm)	196	196	199	197	197	183	169
|Xd|(mm)	4.83	3.84	4.27	6.56	3.08	1.18	1.68
|Rd|(deg)	0.04	3.09	4.18	5.10	0.23	3.32	0.41

FIGURE 3.5: Result of experiment II.

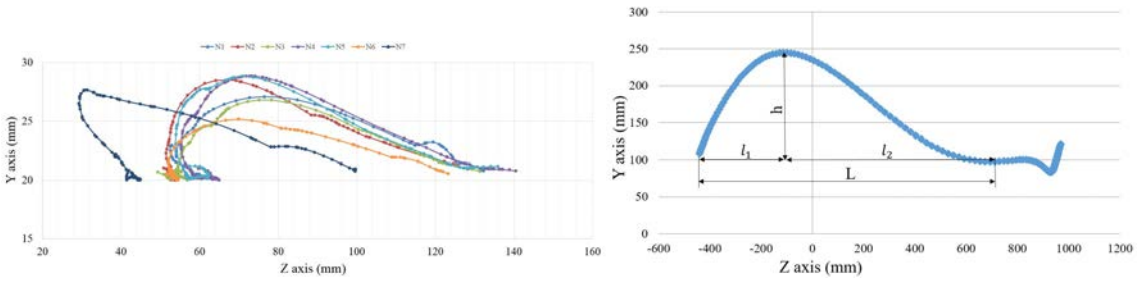

(A) (B)

FIGURE 3.6: Ankle trajectory in a cycle: (a) Robot; and (b) Human subject.

trajectory changes to adapt to the new ankle joint position. N7 position is near the robot's heel and same as the human situation. However, the performance of this model is not good.

Table 3.4 describes dimensions of ankle joint trajectory of all simulations in a cycle, as can be seen that N4 and N5 position in the middle have the best performances which is the most comparable to the human ankle joint trajectory. Thus, these ankle joint positions are selected. The waveform comparison of the gait function assigned to all joints are depicted in Fig. 3.7.

TABLE 3.4: Simulation result of experiment II.

No.	l1 (mm)	l2 (mm)	h (mm)	L (mm)	a=h/L	b=l1/l2
N1	19.2	75.7	7.0	94.9	0.07376	0.25363
N2	15.7	64.3	8.1	80.0	0.10125	0.24417
N3	18.2	64.9	6.8	83.1	0.08183	0.28043
N4	19.2	62.8	8.6	82	0.10488	0.30573
N5	16.6	55.9	8.6	79.5	0.10818	0.29696
N6	15.4	53.1	5.1	68.5	0.07445	0.29002
N7	-14.1	68.9	7.6	54.8	0.13869	-0.20464
Human subject	298.85	10004.64	136.26	1303.49	0.10453	0.29747

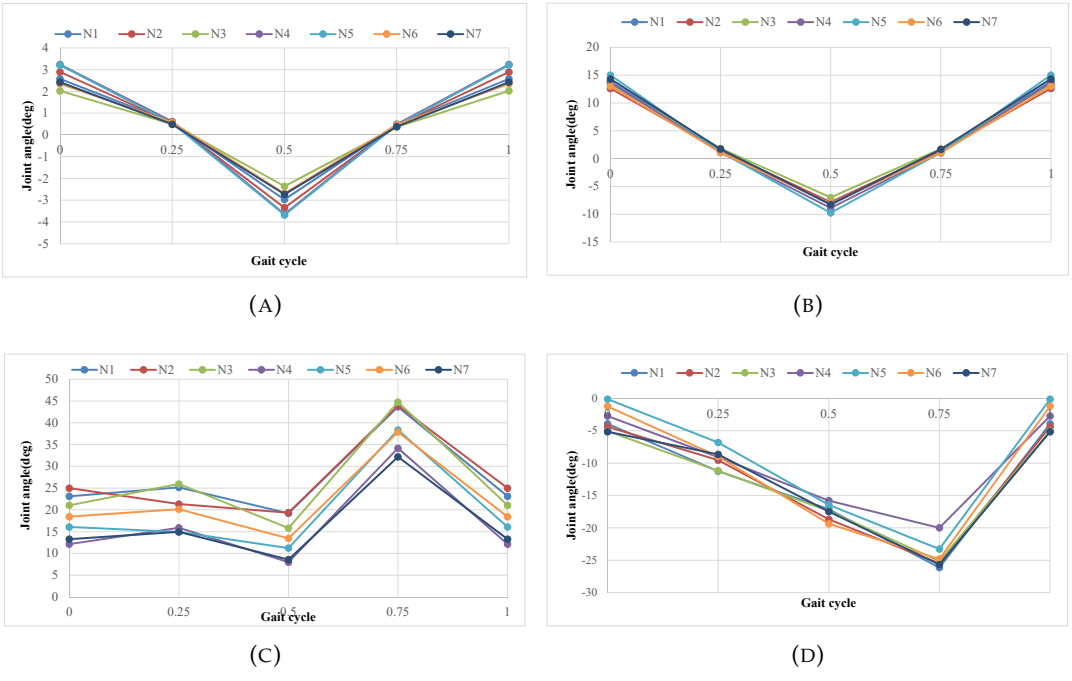

FIGURE 3.7: Waveform of the gait function: (a) Hip and ankle roll joint angle; (b) Hip pitch joint angle; (c) Knee pitch joint angle; and, (d) Ankle pitch joint angle.

When I change the ankle joint position from N1 to N7 as described in Table 3.2, the knee joint angle has gradually declined. The other joint angles change in small amount. Specially, the hip joint angle only has a small change at 0, 0.5, and 1 in a cycle. The ankle pitches joint angle changes at all. Fig. 3.5 shows that model N5 with

the ratio of 0.33 performs the best result.

3.5 Some foot structures with toe mechanism

In this section, I try to use gait pattern described in Figure 2.7 for some foot structure with toe as shown in Figure 3.8 and I name model F7 for the foot structure simulated in [10].

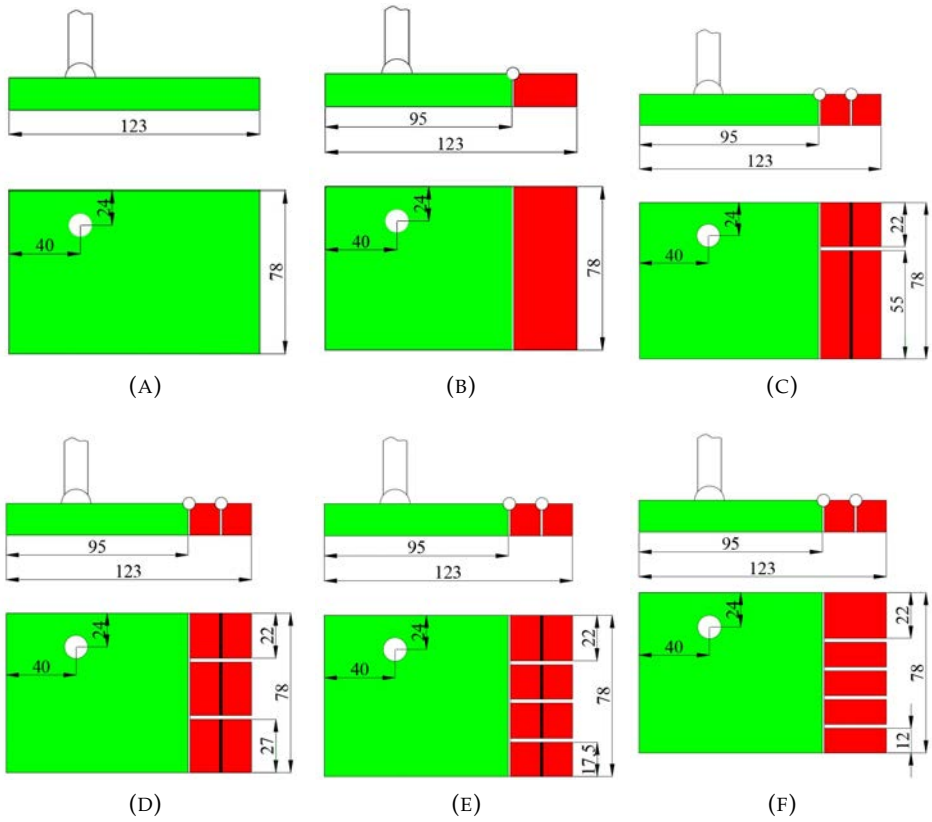

FIGURE 3.8: Foot mechanism with toe: (a) Model F1; (b) Model F2; (c) Model F3; (d) Model F4; (e) Model F5; and, (f) Model F6.

3.5.1 Simulation result on flat ground

In all simulation, I simulate the robot motion in three cycles. One cycle was set up to 1.2s. Thus, three cycles spent on 3.6s. Next, 1.2s was used for checking robot

stability. In this simulation, one step took 0.02s, so the total number of steps was 240. The simulation result is shown Table 3.5. The trajectory of the CoM is depicted

TABLE 3.5: Simulation result on flat ground.

Model	Distance		Rotation
	Lateral (mm)	Walking (mm)	Angle(^{o})
F2	14.910	193.91	-5.867
F3	-28.187	197.76	-9.557
F4	-0.632	192.77	-2.795
F5	9.350	195.31	1.309
F6	0.384	195.19	2.998
F7	-0.007	177.94	-0.091

as in Figure 3.9.

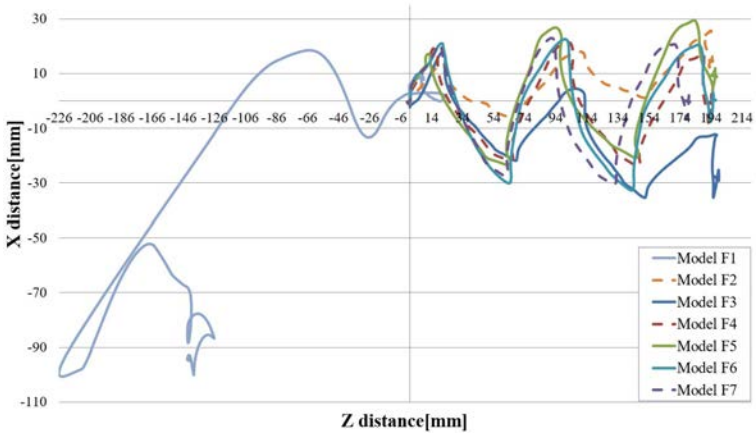

FIGURE 3.9: CoM's trajectory on flat ground.

Model F1 cannot walk with provided control data because this data is generated for foot structure with toe mechanism. Whereas, model F2-F7 can walk normally. In Table 3.5 and Figure 3.9, we see that all the trajectory of the robot's CoG point is approximately the waveform of the circular function which is similar to that of the human's CoM. Maximum walking distance is 197.76mm; side distance is -28.187mm in the case of model F3, is quite large. Thus, consideration of walking straight and

stability, Model F6 with X_f, Y_f, R_f of $0.384mm$, $195.19mm$ and 2.998^o has best performance.

3.5.2 Simulation result on rough ground

This section plans to consider the effect of the foot structures with different toe mechanism on the robot walking behavior with the corrugated ground. I assume that it is normal outdoor road consisting of a positive and a negative wave with the height of 4mm. The length of rough part is 120mm.

In all simulation, the robot motion is simulated in five cycles. One cycle is set up to 1.2 seconds. Thus, five cycles spend on 6.0s. Next, 1.2s is used for checking robot stability. In this simulation, one step takes 0.02 second, so the total number of steps is 360. The simulation result is shown in Table 3.6

TABLE 3.6: Simulation result on rough ground.

Model	Distance		Rotation
	Lateral(mm)	Walking(mm)	Angle(^{o})
F1	-70.85	132.88	-32.22
F2	34.28	301.82	3.98
F3	2.54	298.32	-12.52
F4	-44.55	302.93	-10.66
F5	-124.31	297.81	-35.63
F6	-5.78	311.22	2.79
F7	13.60	293.84	4.29

The trajectory of the CoM point is shown as Figure 3.10.

In Table 3.6 and Figure 3.10, as can be seen that all the trajectory of the robot's CoM are approximately the waveform of the circular function. With the model F1 having no toe mechanism, it is encountered to climb up the obstacles due to the rigid foot structure, thus, walking distance is shortest. By contrast, the robot with toe mechanism can overcome the obstacles comfortably. When the number of toe

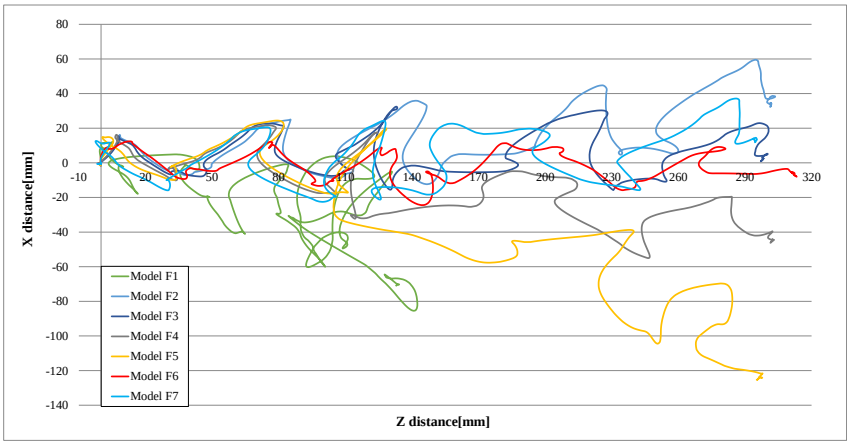

FIGURE 3.10: CoM's trajectory on rough ground.

increases, the foot is more flexible to enhance the number of contact point. Therefore, the robot performs the steady walking. However, in this case, if the toe mechanism has so many passive joints such as model F7, the number of contact point will be excessive, foot gets stuck in concave part of terrain. As a result, the walking distance declines.

The waveform of control data for both of situations are depicted in Fig. 3.11.

3.5.3 Arm Swing Mechanism

As explained in Item 1.5, arm swing motion can preclude ground reaction torque caused by leg swing, thus, F. Naoki's research [11] proposed an arm swing mechanism for the biped robot as depicted in Fig. 3.12. Its principle is similar to a four-bar linkage. The motion of the shoulder joint is provided by the actuator of the contralateral hip pitch joint through two linear springs with damper. My work applies this structure to improve stability of the best model in Item 3.5.2: F6 during walking on rough road. I design it with transmission ratio of 1.67. The stiffness and damping coefficient are set to 0.8 (N/mm) and 0.008 (N.s/mm), respectively. Model F6 is built in two configurations: no arm swing and with arm swing mechanism to observe its

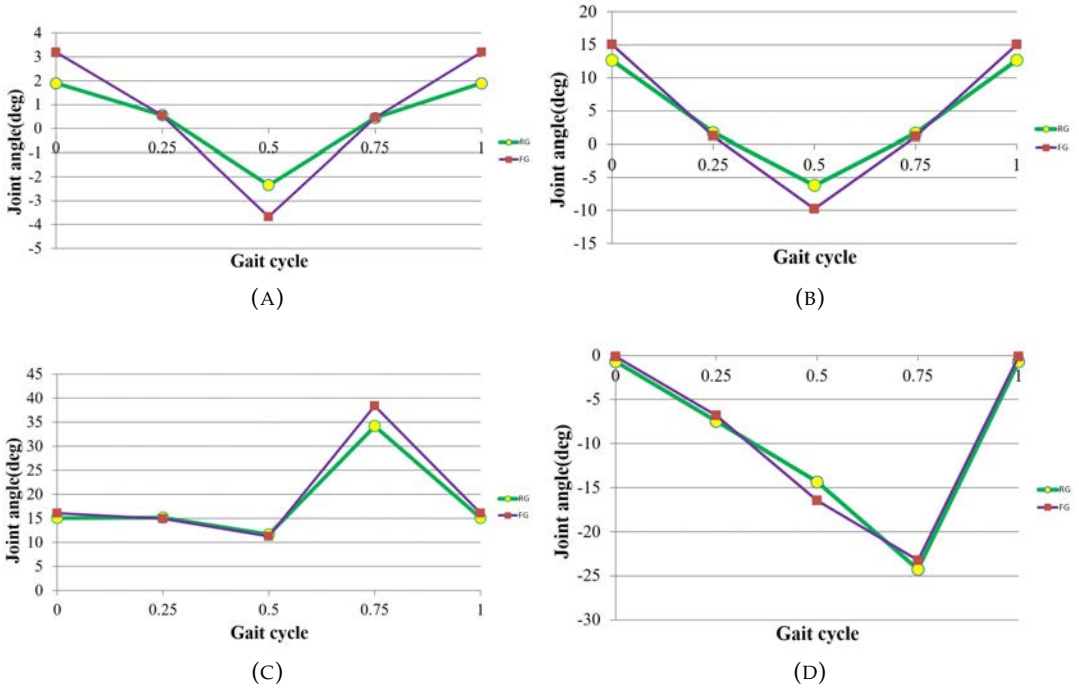

FIGURE 3.11: Waveform of the gait function: (a) Hip and ankle roll joint angle; (b) Hip pitch joint angle; (c) Knee pitch joint angle; and, (d) Ankle pitch joint angle.

behavior as depicted in Figure 3.13.

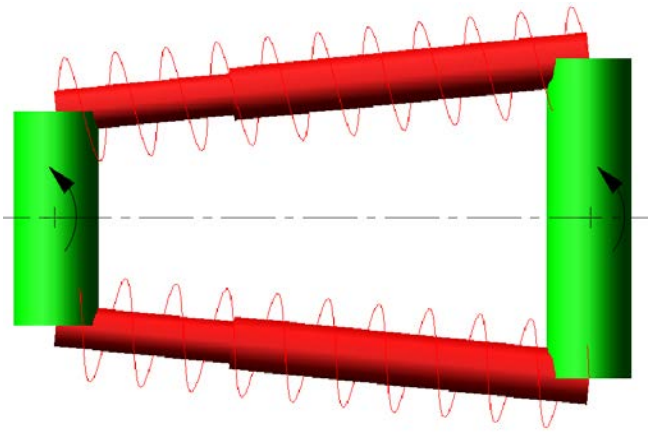

FIGURE 3.12: Arm swing principle of the robot.

To be more comprehensible, I will deploy Figure 1.15 as shown in Figure 3.14 and calculate moment of inertia force exerted by leg and arm swing at time (t)=1.2s

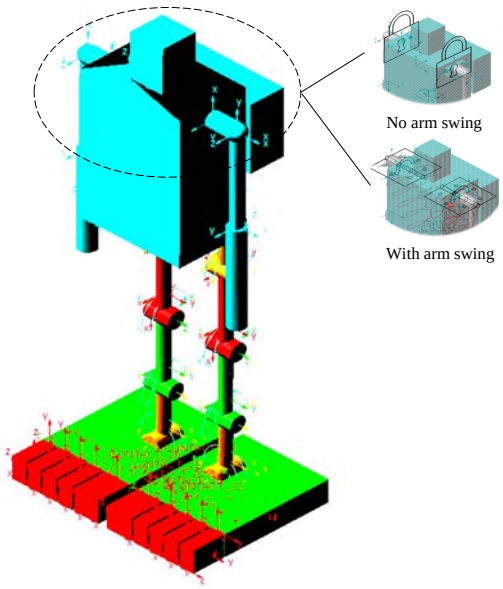

FIGURE 3.13: Model F6 in two configurations: no arm swing and with arm swing mechanism.

as the following:

Moment of inertia force exerted by part swing is

$$M = F.d. \tag{3.1}$$

Where, F is inertia force, d is distance between two parts.

$$F = m.a. \tag{3.2}$$

Where m is weight of part, a is a horizontal part of acceleration calculated by Eq. 3.3

$$a = a_t.cos(\varphi_{max}) + a_n.sin(\varphi_{max}). \tag{3.3}$$

Where a_t, a_n are tangential and centripetal acceleration, respectively. φ_{max} is maximum of angle of rotation. Back to Eq. 2.1.

$$\varphi(t) = a + b.cos(\omega t) + c.sin(\omega t) + d.cos(2\omega t). \tag{3.4}$$

Thus, angular velocity and acceleration of leg are

$$\omega_p = \dot{\varphi}_l(t) = -b.\omega.sin(\omega t) + c.\omega.cos(\omega t) - 2.d.\omega.sin(2\omega t). \tag{3.5}$$

$$\gamma = \ddot{\varphi}(t) = -b.\omega^2.cos(\omega t) - c.\omega^2.sin(\omega t) - 4.d.\omega^2.cos(2\omega t). \tag{3.6}$$

Tangential and centripetal acceleration are

$$a_t = l.\gamma \tag{3.7}$$

$$a_n = \omega_p^2.l \tag{3.8}$$

Where l is distance from center of mass of part to joint, respectively. Replace Eq. 3.5-3.6 to Eq. 3.7- 3.8.

$$a_t = l.\ddot{\varphi}_l(t) = (-b.\omega^2.cos(\omega t) - c.\omega^2.sin(\omega t) - 4.d.\omega^2.cos(2\omega t)).l. \tag{3.9}$$

$$a_n = (-b.\omega.sin(\omega t) + c.\omega.cos(\omega t) - 2.d.\omega.sin(2\omega t))^2.l \tag{3.10}$$

Replace Eq. 3.9- 3.10 to Eq. 3.3- 3.2, horizontal part of acceleration and inertia force are

$$\begin{aligned} a = (-b.\omega^2.cos(\omega t) - c.\omega^2.sin(\omega t) - 4.d.\omega^2.cos(2\omega t))).l.cos(\varphi_{max}) + \\ (-b.\omega.sin(\omega t) + c.\omega.cos(\omega t) - 2.d.\omega.sin(2\omega t))^2.l.sin(\varphi_{max}). \end{aligned} \tag{3.11}$$

$$F = m.l.[(-b.\omega^2.cos(\omega t) - c.\omega^2.sin(\omega t) - 4.d.\omega^2.cos(2\omega t)).cos(\varphi_{max}) + (-b.\omega.sin(\omega t) + c.\omega.cos(\omega t) - 2.d.\omega.sin(2\omega t))^2.sin(\varphi_{max})]. \quad (3.12)$$

Finally, moment of inertia force is

$$M = m.d_1.l.\omega.[-b.\omega.cos(\omega t) - c.\omega.sin(\omega t) - 4.d.\omega.cos(2\omega t)).cos(\varphi_{max}) + (-b.sin(\omega t) + c.cos(\omega t) - 2.d.sin(2\omega t))^2.sin(\varphi_{max})]. \quad (3.13)$$

For the leg, m_{thigh}=0.1(kg), m_{shin}=0.065(kg), d_l=56(mm), l_{thigh}=33(mm), l_{shin}=31(mm), ω=5.236$(1/s)$, t=1.2(s), φ_{max1}=12.63^o, φ_{max2}=21.53^o, a_2= 0.043, b_2= 0.164, c_2= 0.001, d_2= 0.014, a_3= 0.332, b_3= 0.030, c_3= -0.166, d_3= -0.098. Thus, moment of inertia force exerted by leg swing M_l= 1112.36 + 995.66 = 2108.02 $(N.mm)$.

For the arm, because of transmission ratio of 1.67, the angular velocity of rotation of the arm is faster than the leg by 1.67 of times, m_{arm}=0.1(kg), d_a=91(mm), l_{arm}=40(mm), ω=5.236$(1/s)$, t=1.2(s), φ_{max}=25.05^o, a= 0.043, b= 0.164, c= 0.001, d= 0.014. Thus, moment of inertia force exerted by arm swing M_h= 2187.94 $(N.mm)$. This moment have an inverse direction with the one exerted by leg swing. Thus, it precludes an effect of moment of inertia force on the robot, M_e=M_l - M_h= 2108.02 - 2187.94= -79.92 $(N.mm)$

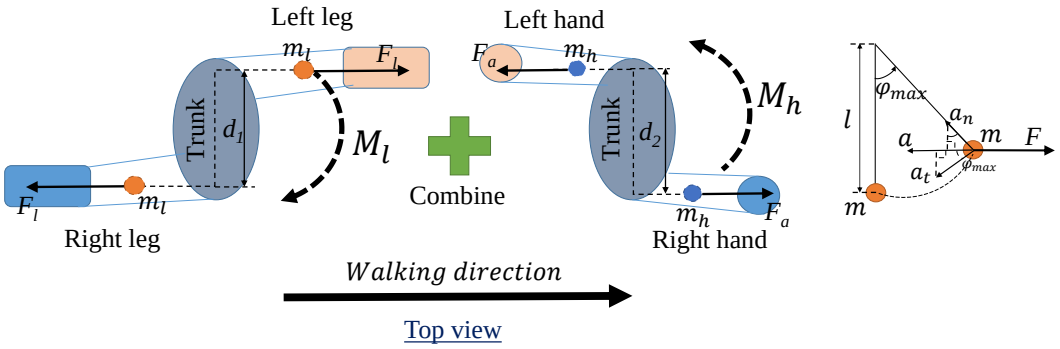

FIGURE 3.14: Moment of inertia force exerted by leg and arm swing.

The simulation result is shown as Figure 3.15. As can be seen that angle of rotation witnesses a significant decrease from 2.79^o to 0.12^o with about 95.7%. Besides, its amplitude of fluctuation goes down from 21.65^o to 20.43^o with around 6%.

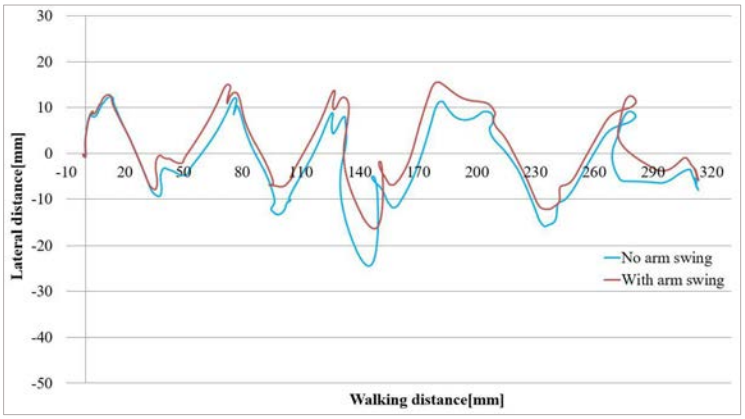

Situation	Walking distance (mm)	Lateral distance (mm)	Angle of rotation (º)
No arm swing	311.22	-5.78	2.79
With arm swing	311.53	-3.60	0.12

(A)

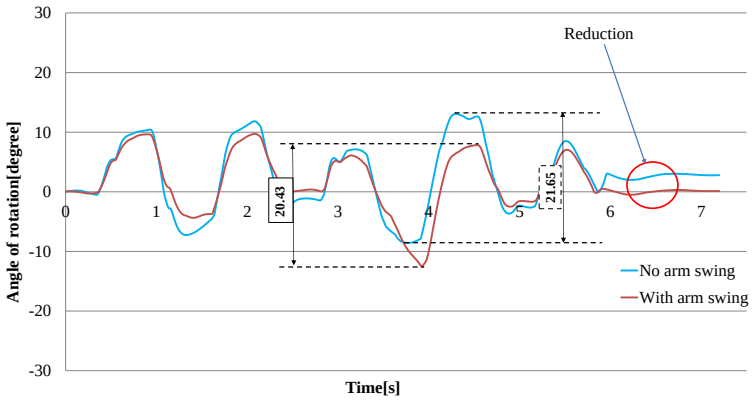

(B)

FIGURE 3.15: Simulation result: (a) CoM trajectory on 4mm wave ground; and (b) Angle of rotation.

3.6 Conclusion

In this chapter, the effects of two robot foot structure parameters are considered. The first experiment result shows that with the novel gait generation method, the big toe's width has no the significant effect on the biped robot walking behavior. Through the second experiment, all the models with changing the ankle joint position can walk straight and stay within the constraint conditions. The robot ankle joint trajectory is compared with that of the human to observe the effect of the ankle joint position on its walking behavior and discover the best one for the ankle joint. Finally, the locomotion of the robot with different toe mechanisms is compared on both types of terrains: flat and rough ground. The simulation shows that foot structure consisting of big and baby toe can overcome 4mm-high wave obstacle and the model having a big toe and 4 baby toes reveals the best performance.

Bibliography

[1] J. Yamaguchi, E. Soga, S. Inoue, and A. Takanishi, “Development of a bipedal humanoid robot-control method of whole body cooperative dynamic biped walking”, Proceedings of the IEEE International Conference on Robotics and Automation (1999), pp. 368–374.

[2] Y. Sakagami, R. Watanabe, C. Aoyama, S. Matsunaga, N. Higaki, and K. Fujimura, “The intelligent ASIMO: System overview and integration”, Proceedings of the IEEE/RSJ International Conference on Intelligent Robots and Systems (2002), pp. 2478-2483.

[3] S. Lohmeier, K. Loffler, M. Gienger, H. Ulbrich, and F. Pfeiffer, “Computer system and control of biped "Johnnie"”, Proceedings of IEEE International Conference on Robotics and Automation (2004), vol. 4, pp. 4222-4227.

[4] T. Ishida, “Development of a Small Biped Entertainment Robot QRIO”, Proceedings of The Fourth Symposium Micro-Nanomechatronics for Information-Based Society (2004), pp. 23-28.

[5] Y. Ogura, H. Aikawa, K. Shimomura, A. Morishima, H.o. Lim, and A. Takanishi, “Development of a new humanoid robot WABIAN-2”, Proceedings of IEEE International Conference on Robotics and Automation (2006), pp. 830-835.

[6] K. Yamane and L. Trutoiu, “Effect of Foot Shape on Locomotion of Active Biped Robots, a study on effect of two-arch structure of foot for biped robots”, Proceedings of 9th IEEE-RAS International Conference on Humanoid Robots (2009), pp.

2230-2236.

[7] R. Sellaouti, O. Stasse, S. Kajita, K. Yokoi, and A. Kheddar, "Faster and smoother walking of Humanoid HRP-2 with passive toe joints", Proceedings of IEEE/RSJ international conference on intelligent robots and systems (2006), pp. 4909-4914.

[8] S. Lohmeier, T. Buschmann, H. Ulbrich, and F. Pfeiffer, "Modular joint design for performance enhanced humanoid robot LOLA", Proceedings of IEEE international conference on robotics and automation (2006), pp. 88-93.

[9] K. Nerakae and H. Hasegawa, "Big toe sizing design of small biped robot by using gait generation method", Applied Mechanics and Materials (2014), vol. 541-542, pp. 1079-1086.

[10] V-T. Nguyen, T. Bui, and H. Hasegawa, "A Gait Generation for Biped Robot Based on Artificial Neural Network and Improved Self-Adaptive Differential Evolution Algorithm", International Journal of Machine Learning and Computing (2016), no.6, vol. 6, pp. 260-266.

[11] F. Naoki, "24 時間の連続稼働を目標とした二足歩行ロボットの省エネルギー化" , Masterś thesis (2017), Shibaura Institute of Technology.

Chapter 4

Walking Behavior of Biped Robot on Rough Road

This chapter addresses a behavior of the biped robot while walking on ground road with an optimal foot structure. It is based on the consideration of four cases where the ground reaction force is set up in different conditions and the optimal foot structure is a combination of topology optimization result of these situations.

4.1 Introduction

With the development of science and technology, the robots are ensuring its indispensable role in human society. In this field, we are not able to omit the humanoid robots which are employed in various applications such as support tasks, entertainment, replacing humans in dangerous tasks, etc.[1]. In this area, the human-like walking has always been the major concern. Until now, the walking problem is still one of the most challenging issues even for a locomotion on a perfectly flat surface where the robot walking is required to be stable and natural like the human beings. This demand comes from the safety and the confidence of the robot in human daily life.

By investigating the papers in the same area, we can mention some highlight researches. For instance, conventional approach which generates the robot motion is based on the zero moment point (ZMP) and foot trajectories is predefined [2, 3, 4]. Simultaneously, a controller is integrated to conserve the balance under internal errors and external disturbances. In these papers, the sole of the feet is used to parallel the ground to make balance easier. However, the human walking is a complicated process which includes two main phases called “stance phase" and “swing phase" [5] as described in Fig. 4.1. When starting a new gait cycle, a foot strikes the ground with its heel and the toe of the stance foot lifts off the ground at the end of the stance phase. These behaviors are named “heel-contact" and “toe-off", respectively, which have an important effect on walking performance since there is a status change of phase in this period.

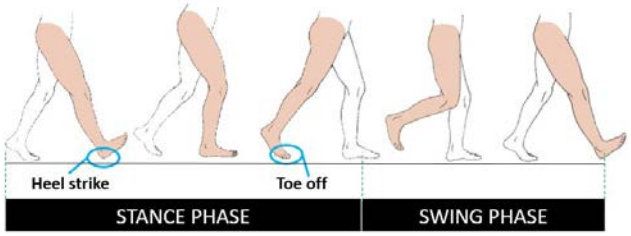

FIGURE 4.1: Human walking behavior in a gait cycle.

From the above-mentioned point of view, a number of the foot structures have been built by analyzing the characteristics of the human foot recently. This approach is a promising way to improve the robot walking behavior. As a result, these researchers achieved the primary success to enhance the robot walking gait toward the human locomotion while focusing on heel strike and toe-off period. In particular, Kouchaki and Sadigh considered the effect of toe-joint bending on biped gait performance [6]. Sadedel et al. added low-cost passive toe joints to the feet structure of SURENA III humanoid robot, using passive toe joints reduced energy consumption of ankle and knee joints in comparison with a similar toe-less robot [7]. In

addition, a human-like ankle-foot complex proposed by Narioka et al. is to imitate a truss mechanism and a windlass mechanism of human beings [8]. Hasegawa and Nerakae proposed a foot structure consist of a big toe and a tiptoe [9]. It enables the foot to increase the contact points and improves the stability.

4.2 Contributions

My research implements to optimize gait behavior of a biped robot while walking on ground road where foot structure proposed by K. Daichi [10] is used. The foot geometry of the robot is built by topology optimization algorithm in which four specific situations are considered. The optimal structure is the combination of four above results. This structure not only reduces the weight of the robot but also ensures its stable walk. In addition, while considering the human walk, I discover that the humans tend to swing their arms. Although the arms play no obvious role in bipedal gait, Hof AL proved that the arm motion aids in recovery of the gait pattern after a perturbation in human normal walking [11]. Thus, in the second part, I applied a mechanism mentioned in [12] to imitate arm swinging motion of the humans for the robot. It can be said that with two applied mechanisms, the robot motion is primarily comparable to the human one. My result is validated by dynamic simulation in Adams environment.

4.3 Structure Description

4.3.1 Introduction to topology optimization

Topology optimization is a computational material distribution method for synthesizing structures without any preconceived shape. This freedom provides topology

optimization with the ability to find innovative, high-performance structural layouts, which has attracted the interest of applied mathematicians and engineering designers.

The conventional topology optimization formulation uses a finite element method [FEM] to evaluate the design performance. The design is optimized using either gradient-based mathematical programming techniques such as the optimality criteria algorithm and the method of moving asymptotes or non gradient-based algorithms such as genetic algorithms.

A topology optimization problem can be written in the general form of an optimization problem as:
Find:

$$x = [x_1, x_2, ..., x_e, ..., x_n]^T$$

Minimize:

$$F = F(u(\rho), \rho) = \int_{\Omega} f(u(\rho), \rho)\ \mathrm{d}V$$

Subject to:

$$G_o(\rho) = \int_{\Omega} \rho\ \mathrm{d}V - V_0 \leq 0$$

$$G_j(u(\rho), \rho) \leq 0\ with\ j = 1, 2, ..., m$$

The problem statement includes the following:

- An objective function F(u(ρ),ρ). This function represents the quantity that is being minimized for best performance. The most common objective function is compliance, where minimizing compliance leads to maximizing the stiffness of a structure.

- The material distribution as a problem variable. This is described by the density of the material at each location ρ(u). Material is either present, indicated by a 1, or absent, indicated by a 0.

- The design space (Ω). This indicates the allowable volume within which the design can exist.
- m constraints G_j(u(ρ),ρ)$\leq$ 0 a characteristic that the solution must satisfy. Examples are the maximum amount of material to be distributed (volume constraint) or maximum stress values.

Evaluating $u(\rho)$ often includes solving a differential equation. Thus, the finite element method is commonly used to do it.

4.3.2 Topology-Based Foot Structure

This study applies the result of K. Daichi's research [10] by considering some situations with different forces as described in Fig. 4.2 and Table 4.1, where the point related to the ankle position of the robot is fixed and the ground reaction forces only act on the supporting point 1, 2 and 3. Since the weight of the robot is 1.5kg, the maximum ground reaction force set to each supporting point is 15N such as case 1, 3 and 4. In case 2, the ground reaction force is equally distributed in three supporting points. To solve this topology optimization problem, the algorithm proposed by Liu and Tovar [13] is applied.

TABLE 4.1: Force distribution.

Case	Force 1[N]	Force 2[N]	Force 3[N]
1	15	0	0
2	5	5	5
3	0	15	0
4	0	0	15

However, in order to reduce the complexity of foot structure since the subject is a small humanoid robot, linear springs are replaced by torsion springs as shown in Fig. 4.3. Optimal foot structure in detail is described in Fig. 4.4. With this topology foot structure, the unnecessary areas are removed, and thus, the weight of the feet is reduced.

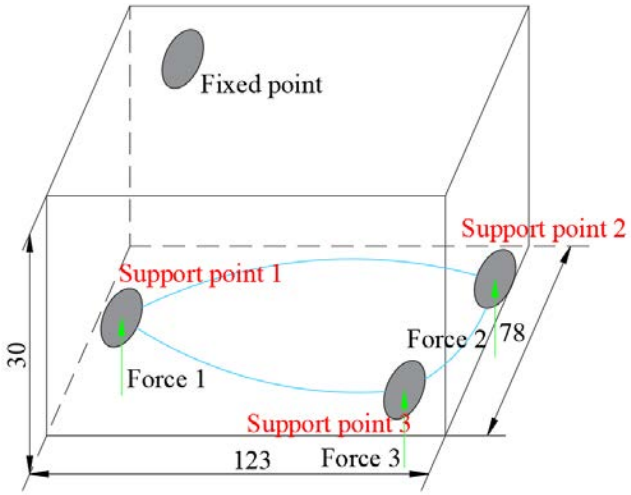

FIGURE 4.2: Design space for topology problem [10].

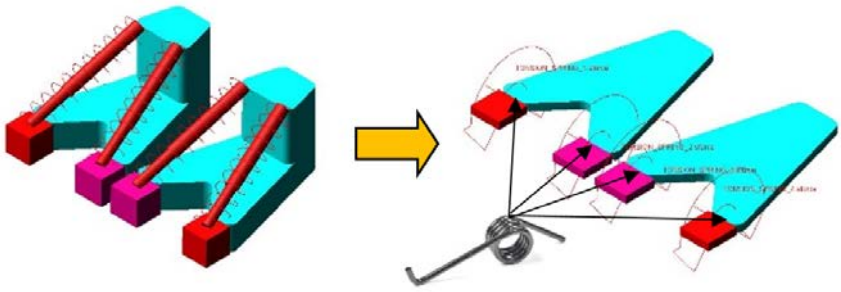

FIGURE 4.3: Optimal foot structure.

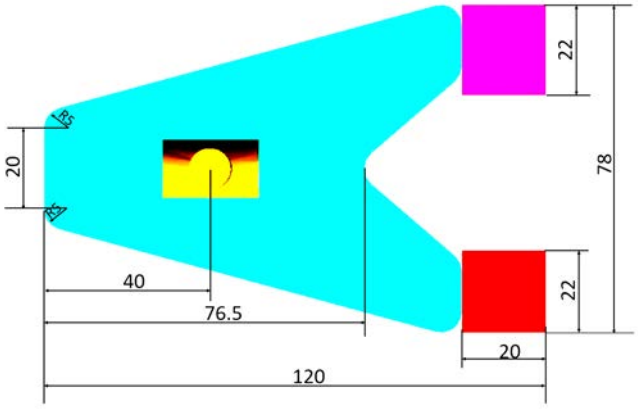

FIGURE 4.4: Design of optimal foot structure.

The walking performance of the robot with the optimal foot structure is illustrated in a cycle described in Fig. 4.5.

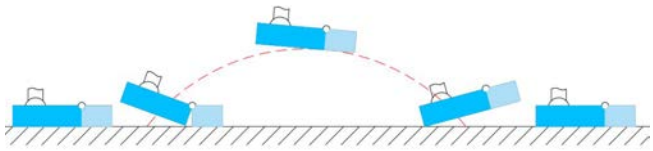

FIGURE 4.5: Adaptive walking behavior.

4.3.3 Backbone structure

The humans' backbone is a complex and functionally significant segment of the human body. Providing the mechanical linkage between the upper and lower extremities, the spine enables motion in all three planes. In humans' walking, the vertebrae flexibly move to maintain the CoM to drop into the support polygon, specially while walking on the rough environment. Thus, the spine has an important role in preserving the humans from falling down.

By above mentioned advantage, F. Naoki [12] introduced a backbone structure using 8 linear springs to constrain the segments of the spine. Based on this idea, I design a simple one consisting of a passive 3-DoF joint and 4 linear springs. When overcoming the obstacles in corrugated ground, the robot's CoM have a trend to move out the polygon support. The spinal motion of the robot keeps CoM point inside the polygon support by moving forward as described in Fig. 4.6a. Backbone structure combining with arm swinging mechanism described in Item 3.5.3 performs upper-body moving behavior as depicted in Fig. 4.6b. It is expected to have a positive effect on locomotion of this robot while walking on high rough level ground.

The stiffness and damping coefficient of all four linear springs are 3.5 N/mm and 0.05 $N.s/mm$, respectively. This mechanism is applied for the robot performance on ground with 10mm-high waves only.

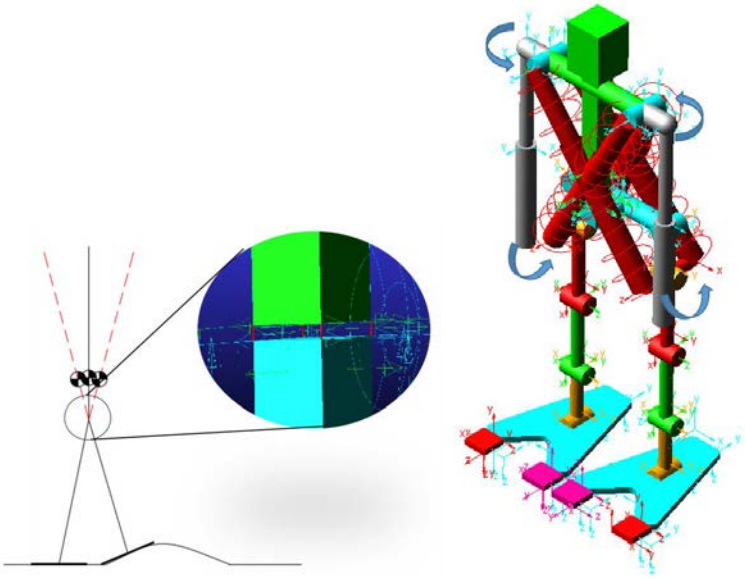

(A) (B)

FIGURE 4.6: Backbone mechanism: (a) Backbone structure; and (b) Upper-body moving behavior.

4.4 Gait function

The joint angles are defined as described in Fig. 4.7, and the range of the angle is based on the human motion data as in Table 4.2.

TABLE 4.2: Range of joint angle.

Angle	View plane	Leg	Joint	Direction	Value
φ_1	Frontal	Both	Hip and ankle	Side to Side	-15^o to 15^o
φ_2	Sagittal	Right	Hip	Extension and Flexion	-50^o to 50^o
φ_3	Sagittal	Right	Knee	Extension and Flexion	0^o to 60^o
φ_4	Sagittal	Right	Ankle	Extension and Flexion	-50^o to 50^o
φ_5	Sagittal	Left	Hip	Extension and Flexion	-50^o to 50^o
φ_6	Sagittal	Left	Knee	Extension and Flexion	0^o to 60^o
φ_7	Sagittal	Left	Ankle	Extension and Flexion	-50^o to 50^o
φ_{8r}	Sagittal	Right	Proximal phalanx	Extension and Flexion	0^o to 30^o
φ_{8l}	Sagittal	Left	Proximal phalanx	Extension and Flexion	0^o to 30^o

In the toe mechanism, since the energy consumption reduction of the robot is considered, the passive joint is selected as a toe joint. Consequently, φ_{8r} and φ_{8l} are

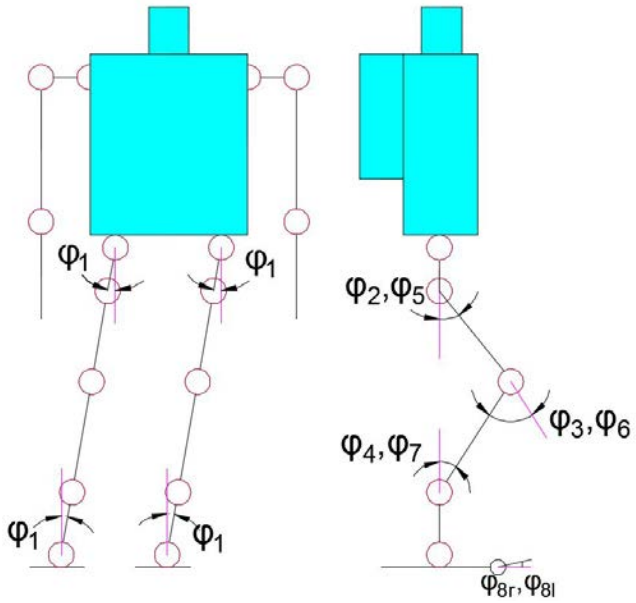

FIGURE 4.7: Robot linkage model.

restricted in (0^o-30^o) range. Their values depend on the robot's geometric posture and the impact forces in its walking process.

4.4.1 Procedure for flat ground

This part is referred to Item 2.2.2 in Chapter 2 with range of design variables is predefined as in Table 4.3.

4.4.2 Procedure for rough ground

The gait functions which are assigned to all joints are described by Eq. 4.1 - Eq. 4.7. Table 4.3 is also used to set a range of design variables for this situation.

$$\varphi_1 = \begin{cases} 0; & t = 0 \; or \; t \geq 8.4 \\ \pm 1.5; & t = 0.3 \; \& \; t = 8.1 \\ \varphi_1(t); & 0.3 < t < 8.1 \end{cases} \quad (4.1)$$

$$\varphi_2 = \begin{cases} 0; & t \leq 0.3 \; or \; t \geq 8.4 \\ \varphi_2(t + 0.6); & 0.3 < t < 8.1 \\ 15; & t = 8.1 \end{cases} \quad (4.2)$$

TABLE 4.3: Range for design variables.

Design variables	Lower boundary	Upper boundary
a_1	0	0.006
b_1	0	0.1
c_1	0	0.002
d_1	-0.01	0
a_2	0	0.08
b_2	0	0.4
c_2	0	0.001
d_2	0	0.02
a_3	0	0.8
b_3	0	0.08
c_3	-0.4	0
d_3	-0.2	0
a_4	-0.4	0
b_4	0	0.3
c_4	0	0.2
d_4	0	0.1

$$\varphi_3 = \begin{cases} 0; & t \leq 0.3 \text{ or } t \geq 8.4 \\ \varphi_3(t+0.6); & 0.3 < t < 8.1 \\ 30; & t = 8.1 \end{cases} \quad (4.3)$$

$$\varphi_6 = \begin{cases} 0; & t = 0 \text{ or } t \geq 8.1 \\ 30; & t = 0.3 \\ \varphi_3(t); & 0.3 < t < 8.1 \end{cases} \quad (4.6)$$

$$\varphi_4 = \begin{cases} 0; & t \leq 0.3 \text{ or } t \geq 8.4 \\ \varphi_4(t+0.6); & 0.3 < t < 8.1 \\ 15; & t = 8.1 \end{cases} \quad (4.4)$$

$$\varphi_7 = \begin{cases} 0; & t = 0 \text{ or } t \geq 8.1 \\ 15; & t = 0.3 \\ \varphi_4(t); & 0.3 < t < 8.1 \end{cases} \quad (4.7)$$

$$\varphi_5 = \begin{cases} 0; & t = 0 \text{ or } t \geq 8.1 \\ 15; & t = 0.3 \\ \varphi_2(t); & 0.3 < t < 8.1 \end{cases} \quad (4.5)$$

4.5 Simulation Results

4.5.1 Flat ground

To apply arm swing mechanism described in Section 3.5.3, I build the simulation model in Adams environment as shown in Fig. 4.8. As can be seen that the robot is considered in two configurations: At first, joint of shoulder is locked or in other words it has no joint. With second configuration, 1-DoF joint is designed for the shoulder.The robot locomotion is simulated on a perfectly flat ground as depicted in Fig. 4.9.

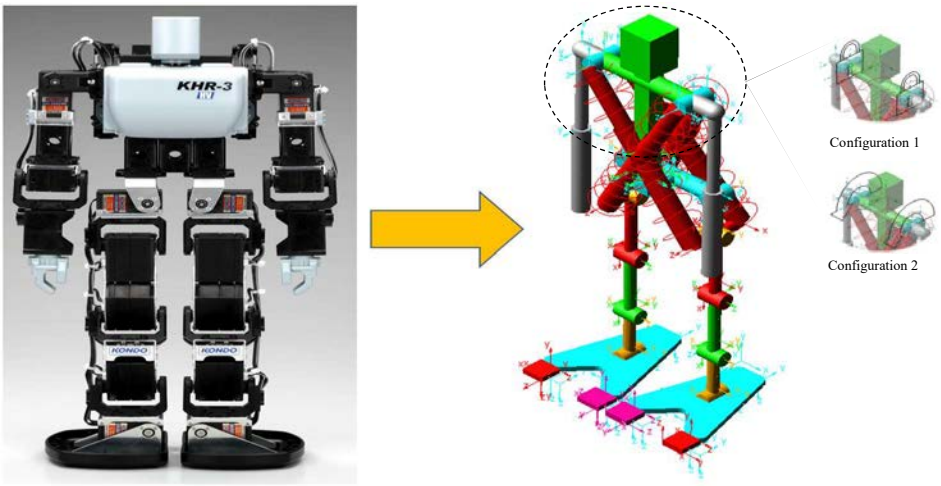

FIGURE 4.8: Real robot and proposed robot.

The optimal value for the design variable is presented in Table 4.4. By returning these coefficients to the gait function described in Eq. 2.1. Four gait functions will be generated to assign to all of joint of the robot, which follows the principle as shown by Eq. 2.2 - Eq. 2.8.

The simulation result shows that X_f lateral distance, Z_f walking distance and R_f angle of rotation are 6.17mm, 172.11mm, and 9.19^o, respectively for configuration 1; 9.99mm, 187.66mm, and 4.18^o, respectively for configuration 2. To be specific, Figure. 4.10a shows that the trajectory of the robot's CoM, which is a periodical wave,

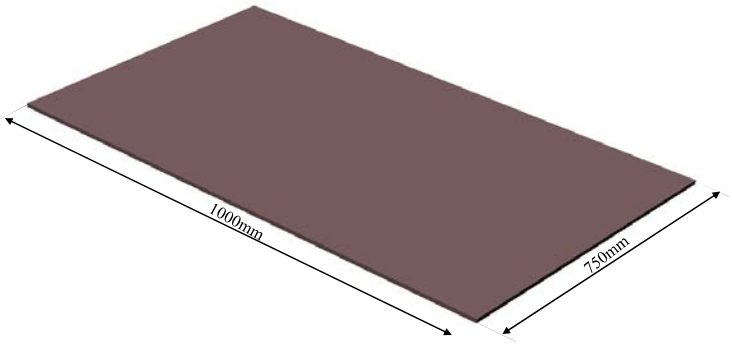

FIGURE 4.9: Flat environment.

TABLE 4.4: Optimal value for design variables on flat ground.

i	Design variables for flat ground			
	a_i	b_i	c_i	d_i
1	0.003	0.045	0.001	-0.007
2	0.041	0.210	0.001	0.013
3	0.414	0.039	-0.189	-0.111
4	-0.245	0.146	0.103	0.049

is comparable to the humans as described in [14]. Figure. 4.10b illustrates the angle of the right foot rotation along the time axis in the walking process. We can see that this angle experiences a fluctuation about from -25^o to 25^o around zero line, which means the feet rotate with a significant amplitude in the locomotion. However, from 3.0s to 3.3s, while the robot prepares to change into a stand, the angle of rotation quickly decreases and this angle is constant in stability checking period. To compare performance of two configuration, we can see that the model having arm swing behavior has better performance. In detail, walking distance experiences an increase of about 9%. In addition, the model having no shoulder joint adopts a little larger fluctuation of angle of rotation and account for 5%, this angle at the final position is decreased by around 55%.

This discussion is to consider walking behavior of the robot in comparison with the human walking process. In Fig. 4.11, the robot walking behavior is depicted

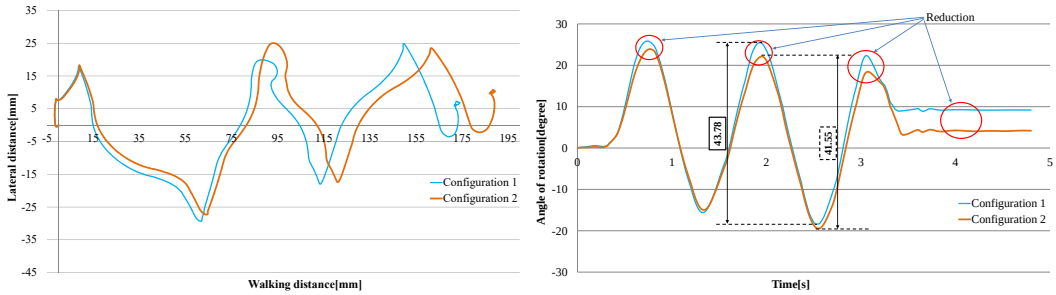

(A) (B)

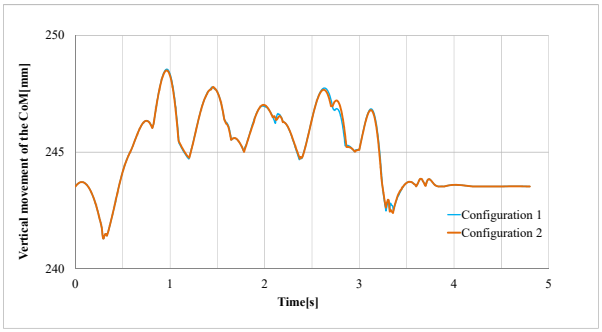

(C)

FIGURE 4.10: Simulation result: (a) CoM trajectory on flat ground; (b) Angle of rotation; and (c) Vertical movement of the CoM.

on the flat ground. A glance at this figure shows that the robot gait which looks like an "Initial contact period" at 1.2s, "Mid-stance period" at 1.5s, "Terminal stance period" at 1.8s, "Initial swing period" at 2.1s, "Terminal swing period" at 2.4s and starting a new cycle. At 1.5s and 2.1s, the bending of toes can be observed clearly, it is toe-off characteristic of the robot which is similar to the human one. This behavior may result in a smooth contact between the robot foot and the ground and play an important role in walking stability. Nevertheless, the heel-strike characteristic is unclear and needed to be improved in the future. Moreover, by inspecting the arm motion, for configuration 1, no arm movement is observed. On the other hand, arms of configuration 2 swing in a pendulum-like motion which is opposite to the contralateral leg motion and therefore precludes the angular momentum of the legs. This leads to improve the stability of the robot in the locomotion.

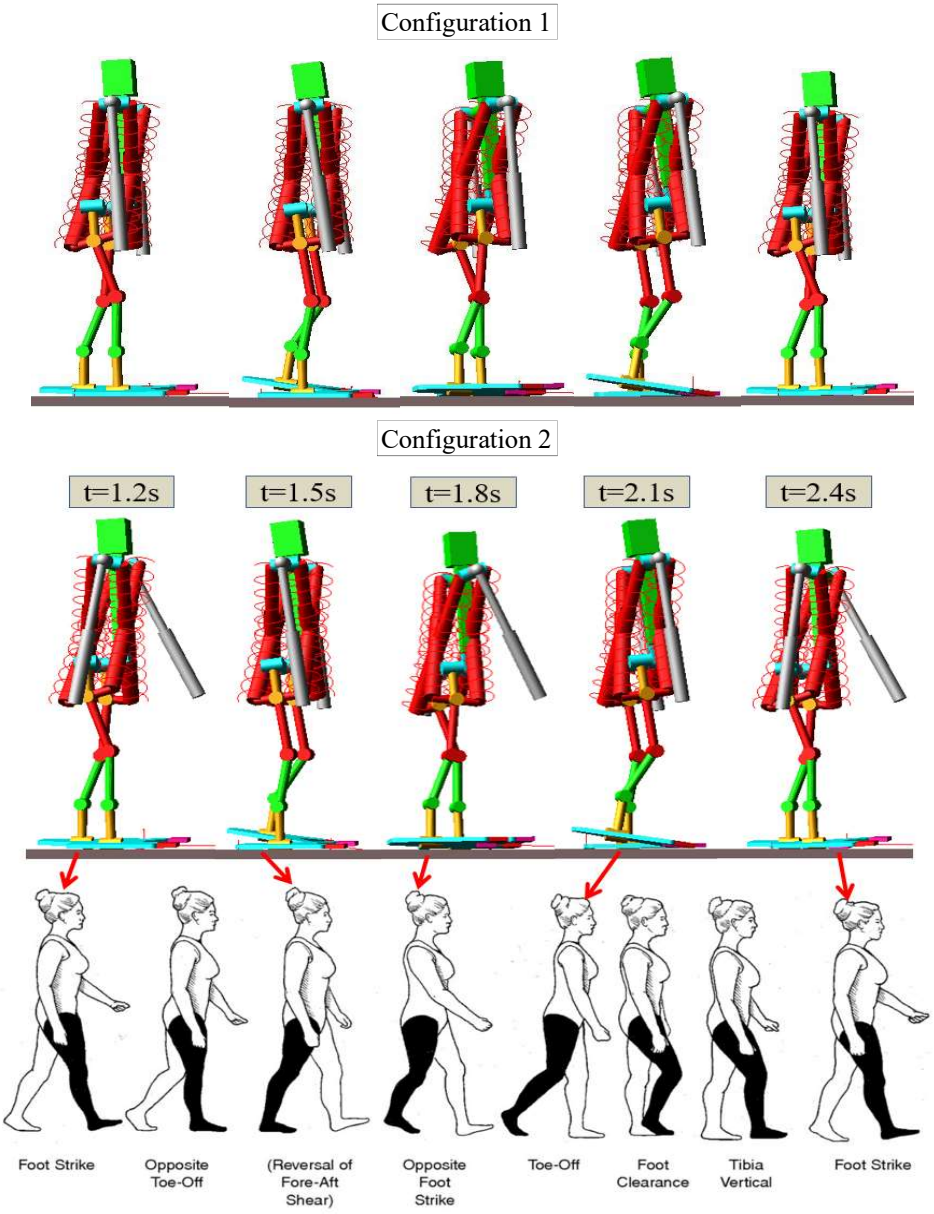

FIGURE 4.11: Robot's CoM trajectory.

The waveform of the gait functions assigned to all joints are depicted in Fig. 4.12. In comparison with the gait pattern of the humans shown in Figure 2.3, it can be seen from Fig. 4.12b and Fig. 4.12c that the hip and the knee gait patterns resemble the gait pattern of the human beings. In Fig. 4.12d, the ankle gait pattern of the robot is

different from the ankle gait pattern of the humans.This difference occurs as result of the physical structure dissimilarity between the robot and the human in ankle joint structure.

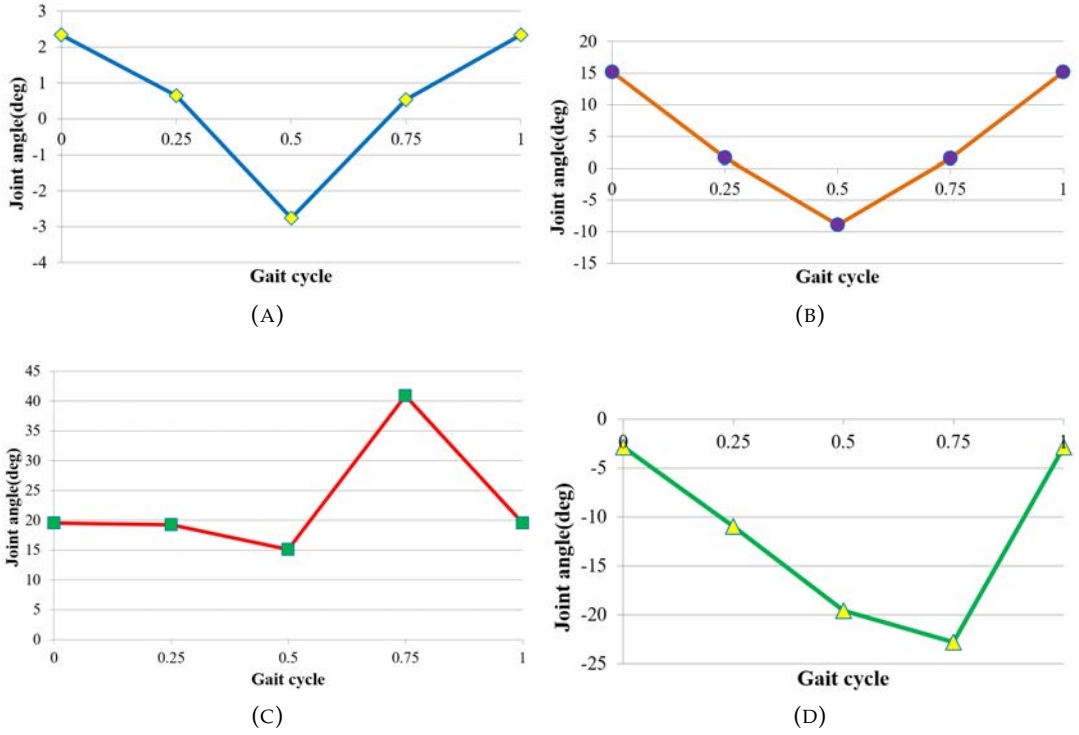

FIGURE 4.12: Waveform of the gait function: (a) Hip and ankle roll joint angle; (b) Hip pitch joint angle; (c) Knee pitch joint angle; and (d) Ankle pitch joint angle.

4.5.2 Rough ground

The ground surface designed for the robot walking performance consists of two parts: Flat and rough surface, the length of the corrugated segment is 120mm and it combines a positive with a negative wave with the height of 6 and 10mm for each situation as presented in Fig. 4.13.

In these simulations, robot motion is simulated in seven cycles. One cycle is set up to 1.2s. Thus, seven cycles spend on 8.4s. Next, 1.2s is used for checking robot stability. One step will take 0.02s, so total number of steps is 480. Coefficients of

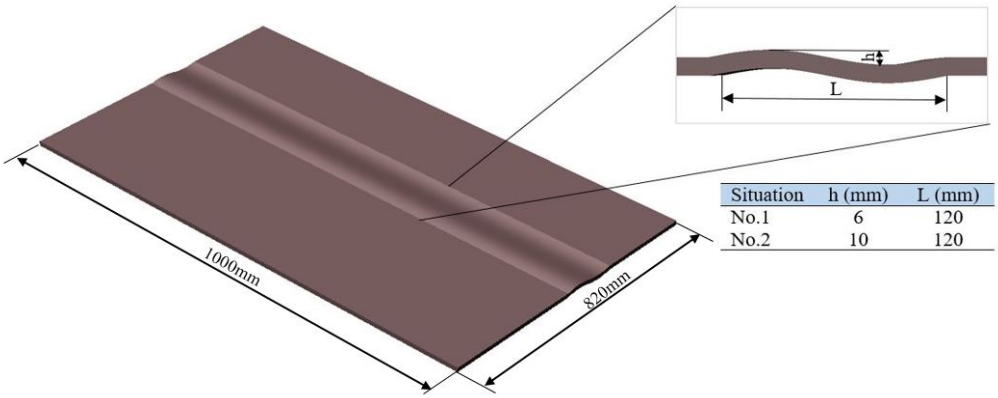

FIGURE 4.13: Rough environment.

the RSM for the first situation are shown in Appendix 1. With 10mm-high wave ground, the RSM and optimization process are not applied because I can not collect enough number of samples for making RSM. The values of design variables on rough ground for both situations are presented in Table 4.5 and the result of simulation is shown in Fig. 4.14.

TABLE 4.5: Value for design variables on rough ground.

i	Design variables for 6mm-high wave ground			
	a_i	b_i	c_i	d_i
1	0.003	0.043	0.001	-0.007
2	0.043	0.204	0.001	0.012
3	0.313	0.032	-0.164	-0.129
4	-0.206	0.129	0.106	0.069
i	Design variables for 10mm-high wave ground			
1	0.003	0.045	0.001	-0.007
2	0.041	0.210	0.001	0.013
3	0.414	0.039	-0.189	-0.111
4	-0.245	0.146	0.103	0.049

In the first configuration, arm wing mechanism is applied only and optimization procedure is implemented to find out the optimal value for design variables. The

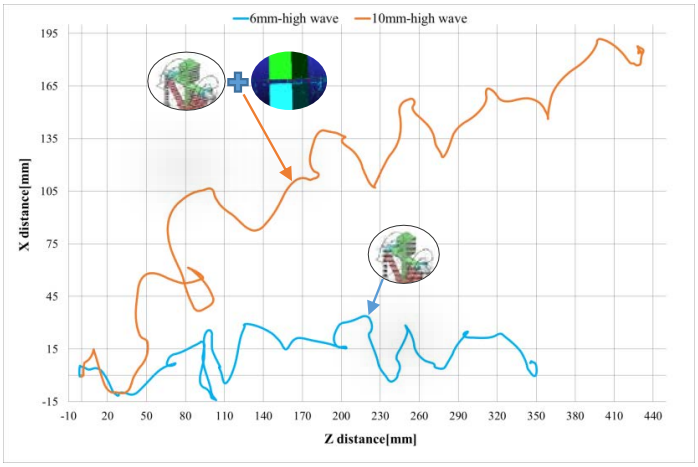

Situation	Walking distance (mm)	Lateral distance (mm)	Angle of rotation (º)
6mm-high wave	346.31	7.77	6.47
10mm-high wave	429.92	184.7	8.46

FIGURE 4.14: Simulation result.

robot walks well and has a good performance on ground with 6mm-high waves. However, when I increase the height of wave, robot can not overcome obstacles and fall down.

In the second configuration, both arm wing mechanism and backbone structure is applied but optimization process has not done because I can not collect enough number of samples. The initial result show that the robot can overcome the 10mm-high waves, however, it still has some limitations. The lateral distance is unexpected big which means the robot does not walk in straight line and the angle of rotation is big as well.

The walking behavior of the robot in the first situation is depicted in Fig. 4.15. As can be seen that, for overcoming the obstacles on the terrain, the robot performs the bending motion of the toe which enhances the contacting points and enable the robot to walk steadily.

The waveforms of the gait functions are depicted in Fig. 4.16.

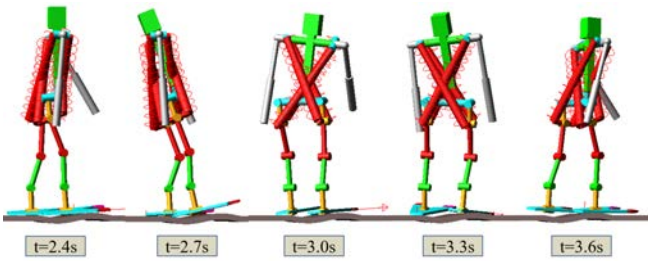

FIGURE 4.15: Robot walking behavior on corrugated ground.

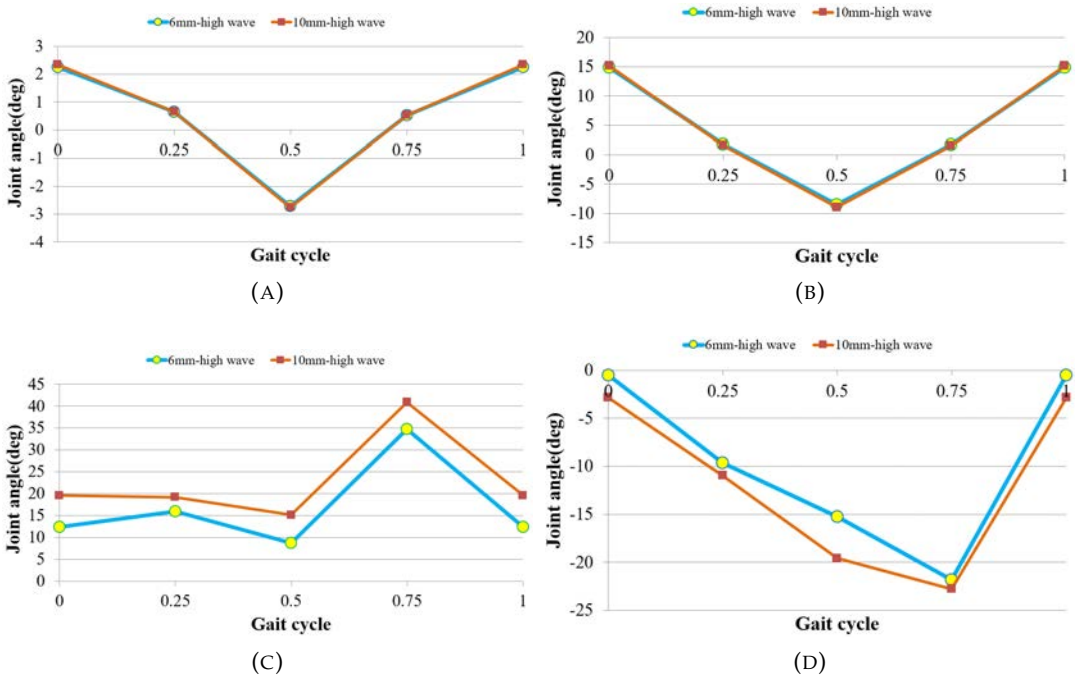

FIGURE 4.16: Waveform of the gait function for walking on rough ground: (a) Hip and ankle roll joint angle; (b) Hip pitch joint angle; (c) Knee pitch joint angle; and, (d) Ankle pitch joint angle.

4.6 Effect of characteristic factors on locomotion on rough road

4.6.1 To introduce Taguchi method

Robust Design method, also called the Taguchi Method, pioneered by Dr. Genichi Taguchi, greatly improves engineering productivity. Taguchi's designs provide a

powerful and efficient method for designing processes that operate consistently and optimally over a variety of conditions. To determine the best design, it requires the use of a strategically designed experiment, which exposes the process to various levels of design parameters.

The design of experiment (DOE) is one of the most powerful tools for experimental planning. It can be used as a great advantage to reduce experimental design changes and cost, as well as to increase design process speed by using statistical methods. The Taguchi method applies an orthogonal array DOEs and selects a large number of control factors with a reduced number of experiments. In this array, the control factor matrix ensures a balanced contrast between the level and independent distribution among parameters. DOE can play an effective role in identifying impacts of many individual parameters on the system performance. The study of the effect of individual parameter can determine the most influential parameters for the performance measure. For more details, the Taguchi concepts and methodologies can be found in [15].

4.6.2 To consider an effect of characteristic factors

In this section, the Taguchi method is applied to consider the effect of four characteristic factors on walking performance of robot while moving on 6mm-high wave ground. These factors are investigated in three levels as described in Table 4.6.

TABLE 4.6: characteristic factors.

Factor		**Design variables**		
		1	2	3
Torsion spring	Stiffness 1(newton.mm/rad) (A)	1.5	2.0	2.5
	Damping 2(newton-mm-sec/rad) (B)	10	20	30
Linear spring	Stiffness 3(newton/mm) (C)	0.6	0.8	1.0
	Damping 4(newton-sec/mm) (D)	0.004	0.008	0.012

Output:

- ◇ Lateral distance: X (mm)
- ◇ Angle of rotation: R (degree)

Design of the orthogonal array I selected L_9 as shown in Table 4.7

TABLE 4.7: Design of experiment.

Orthogonal Array					Result	
No.	A	B	C	D	X (mm)	R (degree)
1	1.5	10	0.6	0.004	-220.77	31.31
2	1.5	20	0.8	0.008	1.61	15.03
3	1.5	30	1.0	0.012	-202.36	-42.93
4	2.0	10	0.8	0.012	28.37	53.79
5	2.0	20	1.0	0.004	-208.73	-20.08
6	2.0	30	0.6	0.008	130.18	52.74
7	2.5	10	1.0	0.008	-184.83	-26.15
8	2.5	20	0.6	0.012	294.58	80.66
9	2.5	30	0.8	0.004	-22.96	29.06

DOF of the entire experiment: DOF = 9 - 1= 8. MSD denotes mean squared deviation calculated by Eq. 4.8. The smaller is better quality characteristic:

$$MSD = (Y_1^2 + Y_2^2 + ... + Y_n^2)/N \tag{4.8}$$

Where Y_i denotes output value, N is a number of run for each experiment. The result of analysis of variance (ANOVA) as shown in Table 4.8- 4.9.

With definitions as below: Where S, S', V, P are functions of Y_i and f.

As can be seen that in case of X output, C has the most significant effect on lateral distance accounting for 45.23%, followed by D with 22.48% and A with 18.01%. B reveals the lowest number with 14.27%. Table 4.9 show that in case of R output, C also has the most significant effect on angle of rotation accounting for 83.54%,

TABLE 4.8: ANOVA with X output.

Factor	f	S	V	S′	P
A	2	46114.80	23057.40	46114.80	18.01
B	2	36539.37	18269.68	36539.37	14.27
C	2	115798.87	57899.44	115798.87	45.23
D	2	57563.34	28781.67	57563.34	22.48
Total	8	256016.38			100.00

TABLE 4.9: ANOVA with R output.

Factor	f	S	V	S′	P
A	2	1481.06	740.53	1481.06	10.72
B	2	225.62	112.81	225.62	1.63
C	2	11544.47	5772.23	11544.47	83.54
D	2	568.48	284.24	568.48	4.11
Total	8	13819.63			100.00

S: Sum of squares
V: Mean squares (variance)
f: Degrees of freedom
S′: Pure sum of squares
P: Percentage by contribution

followed by A with 10.72%, D with 4.11%. B reveals the lowest number with make up only 1.63%. The Fig. 4.17- 4.18 describe the relationship between output and four considered characteristic factors.

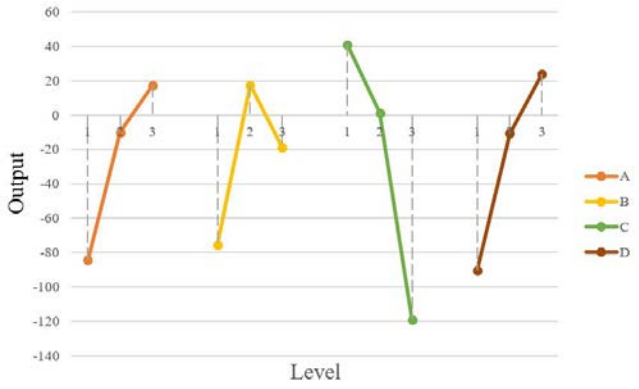

FIGURE 4.17: Relationship between X output and characteristic factors.

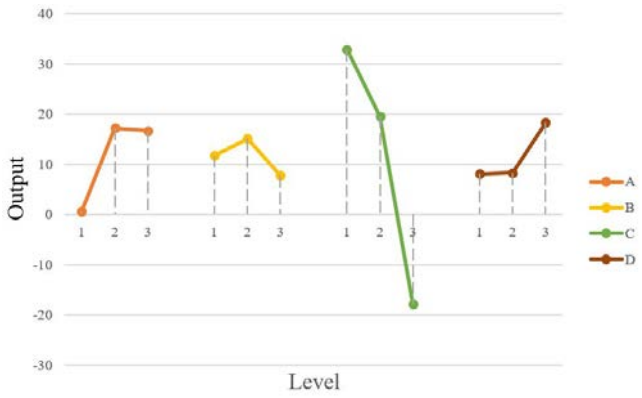

FIGURE 4.18: Relationship between R output and characteristic factors.

4.7 Conclusion

This section is to study on walking behavior of the small biped robot on rough road considering a topology-based foot structure. This structure is a combination of the optimal results when solving four topology problems in which the impact forces is considered in different situations. The optimal design helps reduce the weight of the robot by removing the unnecessary areas of the foot during walking. In addition, the authors also applies the arm swing mechanism to enable the robot to walk naturally and steadily. A gait control data is automatically generated by solving the optimization problem in which ISADE algorithm is applied to the objective function approximated by RSM. The result is validated through dynamic simulation in Adams environment. I confirmed that with the optimal foot structure, the robot walks stably and steadily on the 6mm-high wave ground. In next stage, the Taguchi method is applied to evaluate the effect of four characteristic factors of spring on the walking performance of the robot. The analysis results show that stiffness of linear spring has the most significant effect on straight walk.

Bibliography

[1] K. Tanie, “Humanoid Robot and its Application Possibility”, Proceedings of IEEE International Conference on Multisensor Fusion and Integration for Intelligent Systems (2003), pp. 213–214.

[2] http://kondo-robot.com/product /khr-3hv-ver-2-life (Accessed: 30 May 2016).

[3] K. Muecke and D. Hong, “Constrained analytical trajectory filter for stabilizing humanoid robot motions”, Intelligent Service Robotics (2011), vol. 4, pp. 203-218.

[4] S. Kajita, K. Kaneko, F. Kaneiro, K. Harada, M. Morisawa, S. Nakaoka, K. Miura, K. Fujiwara, E. S. Neo, I. Hara, K. Yokoi, and H. Hirukawa, “Cybernetic Human HRP-4C: A humanoid robot with human-like proportions”, Robotics Research (2011), pp. 301–314.

[5] D. Torricelli, J. Gonzalez, M. Weckx, R. Jiménez-Fabián, B. Vanderborght, M. Sartori, S. Dosen, D. Farina, D. Lefeber, and J.L. Pons, “Human-like compliant locomotion: State of the art of robotic implementations”, Bioinspiration and Biomimetics (2016), no. 5, vol. 11.

[6] E. Kouchaki and M. J. Sadigh, “Effect of toe-joint bending on biped gait performance”, Proceedings of the IEEE International Conference on Robotics and Biomimetics (2010), pp. 697-702.

[7] M. Sadedel, A. Yousefi-Koma, M. Khadiv, and M. Mahdavian, “Adding low-cost passive toe joints to the feet structure of SURENA III humanoid robot”, Robotica, pp. 1-23.

[8] K. Narioka, T. Homma, and K. Hosoda, “Humanlike ankle-foot complex for a biped robot”, Proceedings of the 12th IEEE-RAS International Conference on Humanoid Robots (2012), pp. 15-20.

[9] K. Nerakae and H. Hasegawa, “Big toe sizing design of small biped robot by using gait generation method”, Applied Mechanics and Materials (2014), vol. 541-542,pp. 1079-1086.

[10] K. Daichi, “不整地での歩行安定を目的とした2足歩行ロボット部の最適化”, Masterś thesis (2016), Shibaura Institute of Technology.

[11] A. Hof, “The equations of motion for a standing human reveal three mechanisms for balance”, Journal of Biomechanics (2014), vol. 40, pp. 451-457.

[12] F. Naoki, “24 時間の連続稼働を目標とした二足歩行ロボットの省エネルギー化” , Masterś thesis (2017), Shibaura Institute of Technology.

[13] K. Liu, and A. Tovar, “An efficient 3D topology optimization code written in Matlab”, Structural and Multidisciplinary Optimization (2014), vol. 50, pp. 1175-1196.

[14] M. S. Orendurff, A. D. Segal, J. S. Berge, K. C. Flick, D. Spanier, and G. K. Klute, “The kinematics and kinetics of turning: limb asymmetries associated with walking a circular path”, Gait and Posture (2006), vol. 23, pp. 106-111.

[15] R. K. Roy, “A Primer on the Taguchi Method”, Society of Manufacturing Engineers (1990).

Chapter 5

Conclusions and Future Works

5.1 Conclusions

This research studied on the gait generation method for the biped robot while considering a foot structure having toe mechanism. The main objective is to generate a gait pattern which enables the Kondo KHR-3HV robot to walk naturally on flat and rough road. In addition, this work applies an arm swing mechanism to improve stability of the robot in locomotion.

In my research, there are four simulations to achieve the objective.

In the first simulation, the walking behavior of robot with big toe and tiptoe was investigated by changing the big toe's width. Gait pattern for left leg are generated by four gait functions which are defined by solving constrained optimization problem using ISADE and RSM. For right leg, the gait pattern derives from the data of left one at delayed time of 0.6s. From the result of simulation in Adams environment, I confirm that it can generate successfully a gait pattern for walking process of the robot. Besides, the result show that with a new gait generation method, big toe's width have no significant effect on walking behavior of the robot on flat ground.

In the next simulation, I have investigated some ankle joint positions to determine the best position with the objective of going straight and maximum distance. The result shows that with designed configuration of the robot, ankle joint position

is one third of foot.

Continuously, with selected big toe's width and ankle position, I consider walking behavior of the robot with different foot structures on flat and rough road. As a result, the model having only tiptoe is unable to walk on 4mm-high wave ground. Meanwhile, the model consisting of big and baby toes overcomes this challenge. The foot consisting of one big toe and four baby toes has the best performance. Next, arm swing mechanism is applied to enhance walking behavior on road rough.

The final section considers a foot design based on topology optimization to improve robot walking behavior on 6mm and 10mm-high rough road. The result shows that the robot walk on 6mm-high wave ground comfortably. However, for motion on 10mm-high wave terrain, the applied foot structure still have a limitation. In this section, effect of spring characteristic factors on locomotion is also evaluated by Taguchi method, the result shows that stiffness of linear spring has the most significant effect on straight walk and angle of rotation.

All the simulations are implemented in Adams environment.

5.2 Future works

5.2.1 Flexible foot structure

The human foot has an arch-type skeletal structure which connects heel, toe, and ankle, where the large bone at the heel called calcaneus support about one third of the load and the metatarsal bones connected to the toes absorb the other impact force from the ground [1]. Based on this analysis, I propose a flexible foot structure for the robot as Figure 5.1. This structure consists of 4 wheels and torsion springs to well adapt to an uneven terrain. Four wheels is to reduce the fiction force between sole of the foot and the ground while walking.

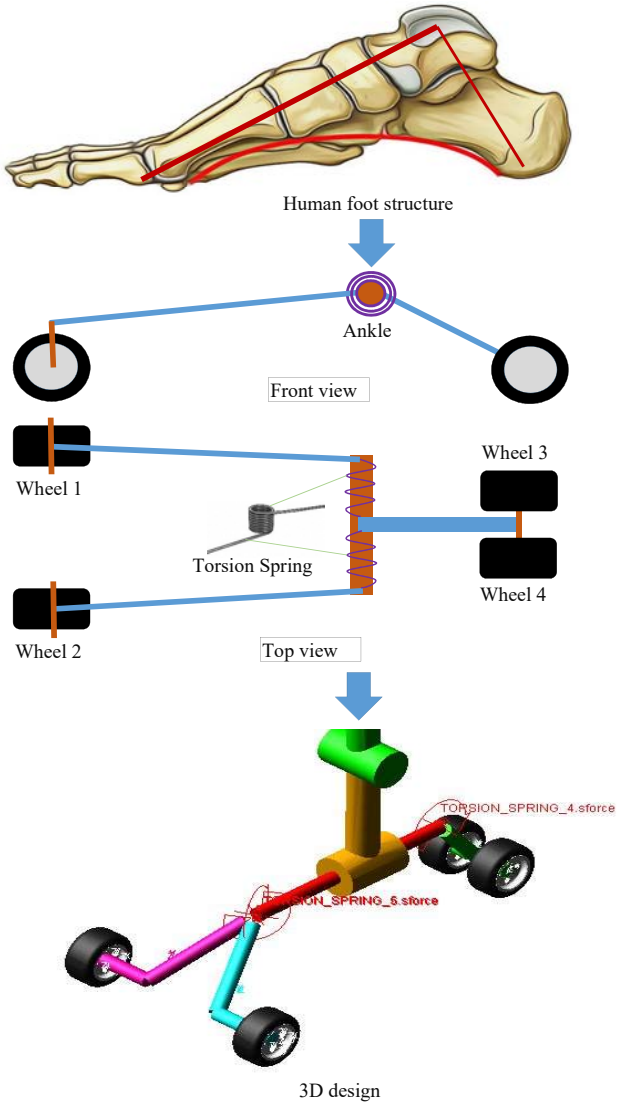

FIGURE 5.1: Flexible foot structure.

5.2.2 Rotation of pelvic

During each stride the pelvis moves asynchronously in all three directions. The site of action is the supporting hip joint. All the motion arcs are small. Researches on human gait's analysis show that the pelvis motion plots in the steady walking phase and plays a significant role in human's gait [2, 3]. Taking into account the results of these researches, I am planning to develop a 1-DOF pelvic for my model as shown

in Fig. 5.2

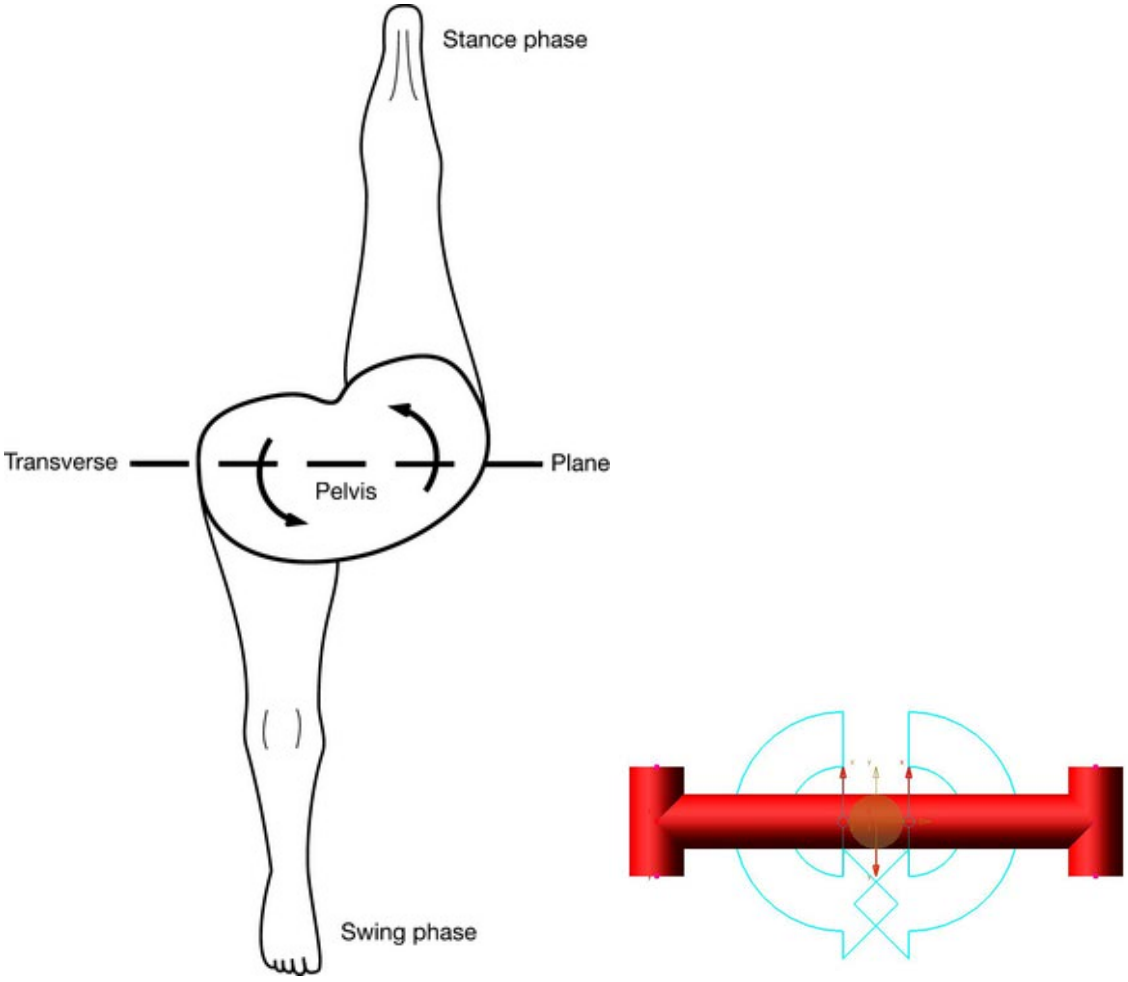

(A) (B)

FIGURE 5.2: Proposed pelvic structure: (a) Human; and (b) 1-DOF pelvic model of robot.

Bibliography

[1] W. Kim, and S. Voloshin, “Role of plantar fascia in the load bearing capacity of the human foot”, Journal of Biomechanics (1995), Vol. 28(9), pp. 1025-1033.

[2] P. E. Klopsteg, and P. D. Wilson, “Human Limbs and Their Substitutes”, New York Hafner (1963).

[3] J. Perry and J. M. Burnfield, “Gait Analysis: Normal and Pathological Function”, 2nd ed., SLACK Incorporated (2010).

Appendix 1

TABLE 5.1: Polynomial coefficients of RSMs for situation of 6mm-high-wave ground

i	Term	Polynomial Coefficients		
		$RSM_Z/10^{11}$	$RSM_X/10^{10}$	$RSM_R/10^9$
1	a_0	70.54	-45.63	-3.27
2	b_1	56.27	-21.10	-1.78
3	b_2	-22.39	7.69	0.67
4	b_3	-26.75	19.76	1.37
5	b_4	62.96	-31.50	-2.41
6	b_5	67.12	-43.56	-3.11
7	b_6	-139.50	78.05	5.81
8	b_7	-58.98	37.55	2.69
9	b_8	-16.04	7.28	0.57
10	b_9	40.25	-22.29	-1.65
11	b_{10}	-55.09	23.99	1.93
12	b_{11}	22.08	-12.75	-0.94
13	b_{12}	-43.43	27.35	1.96
14	b_{13}	13.58	4.34	0.07
15	b_{14}	-11.12	12.26	0.78
16	b_{15}	42.33	-25.84	-1.87

* To be continued *

TABLE 5.1: (continued)

i	Term	Polynomial Coefficients		
		$RSM_Z/10^{11}$	$RSM_X/10^{10}$	$RSM_R/10^9$
17	b_{16}	-22.43	9.93	0.78
18	c_{11}	-7.36	0.01	0.07
19	c_{22}	-1.03	1.28	0.08
20	c_{33}	38.40	-15.97	-1.30
21	c_{44}	0.69	3.66	0.18
22	c_{55}	-39.66	16.67	1.39
23	c_{66}	-10.99	0.24	0.14
24	c_{77}	-35.88	15.59	1.24
25	c_{88}	-75.25	43.37	3.19
26	c_{99}	10.63	-13.77	-0.86
27	c_{1010}	92.14	-53.99	-3.96
28	c_{1111}	12.65	-2.86	-0.30
29	c_{1212}	33.94	-27.56	-1.87
30	c_{1313}	-1.84	6.61	0.38
31	c_{1414}	-23.69	9.03	0.76
32	c_{1515}	31.28	-14.27	-1.12
33	c_{1615}	6.09	-5.20	-0.35
34	c_{12}	21.41	-8.12	-0.68
35	c_{13}	76.60	-42.49	-3.18
36	c_{14}	124.36	-59.96	-4.66
37	c_{15}	70.96	-43.87	-3.17
38	c_{16}	5.06	-5.16	-0.33
39	c_{17}	-33.09	17.85	1.33

* To be continued *

TABLE 5.1: (continued)

i	Term	Polynomial Coefficients		
		$RSM_Z/10^{11}$	$RSM_X/10^{10}$	$RSM_R/10^9$
40	c_{18}	-34.70	18.57	1.40
41	c_{19}	-72.76	33.24	2.62
42	c_{110}	-57.48	29.70	2.26
43	c_{111}	-25.11	13.38	1.01
44	c_{112}	-2.22	-0.17	0.01
45	c_{113}	-9.17	6.06	0.43
46	c_{114}	14.58	-2.83	-0.32
47	c_{115}	-3.20	1.03	0.09
48	c_{116}	-52.88	32.30	2.34
49	c_{23}	-47.59	26.21	1.96
50	c_{24}	-6.27	3.55	0.26
51	c_{25}	102.20	-57.69	-4.28
52	c_{26}	22.42	-11.42	-0.88
53	c_{27}	-14.55	7.90	0.59
54	c_{28}	-32.20	19.71	1.43
55	c_{29}	-4.79	5.82	0.36
56	c_{210}	-16.55	7.17	0.58
57	c_{211}	8.50	-10.99	-0.69
58	c_{212}	-21.65	13.51	0.97
59	c_{213}	44.91	-28.64	-2.06
60	c_{214}	110.73	-68.44	-4.95
61	c_{215}	21.38	-7.00	-0.63
62	c_{216}	-83.27	42.13	3.22

* To be continued *

TABLE 5.1: (continued)

i	Term	Polynomial Coefficients		
		$RSM_Z/10^{11}$	$RSM_X/10^{10}$	$RSM_R/10^9$
63	c_{34}	30.37	-9.64	-0.86
64	c_{35}	11.54	-8.12	-0.58
65	c_{36}	-41.51	20.66	1.59
66	c_{37}	-45.84	22.52	1.73
67	c_{38}	-82.93	45.19	3.38
68	c_{39}	-57.89	34.78	2.53
69	c_{310}	15.88	-7.29	-0.57
70	c_{311}	36.73	-22.18	-1.61
71	c_{312}	-2.84	-2.93	-0.12
72	c_{313}	-61.59	37.79	2.73
73	c_{314}	12.70	-5.96	-0.46
74	c_{315}	95.52	-52.91	-3.96
75	c_{316}	90.83	-50.12	-3.75
76	c_{45}	-40.27	25.00	1.81
77	c_{46}	-15.56	9.56	0.69
78	c_{47}	-63.80	32.67	2.49
79	c_{48}	-43.40	26.21	1.91
80	c_{49}	1.20	5.59	0.29
81	c_{419}	-51.18	27.42	2.08
82	c_{411}	139.38	-81.97	-6.00
83	c_{412}	34.67	-28.08	-1.93
84	c_{413}	29.55	-15.36	-1.16
85	c_{414}	26.26	-8.76	-0.77

* To be continued *

TABLE 5.1: (continued)

i	Term	Polynomial Coefficients		
		$RSM_Z/10^{11}$	$RSM_X/10^{10}$	$RSM_R/10^9$
86	c_{415}	42.77	-22.77	-1.71
87	c_{416}	-30.74	19.93	1.42
88	c_{56}	5.55	-5.27	-0.35
89	c_{57}	-8.44	6.31	0.44
90	c_{58}	-31.41	13.26	1.07
91	c_{59}	-23.00	6.62	0.62
92	c_{510}	11.56	-7.01	-0.51
93	c_{511}	15.42	-9.62	-0.70
94	c_{512}	37.77	-18.51	-1.43
95	c_{513}	-8.39	3.57	0.29
96	c_{514}	-12.51	5.85	0.46
97	c_{515}	-19.51	19.56	1.29
98	c_{516}	1.94	-0.84	-0.07
99	c_{67}	38.60	-16.64	-1.34
100	c_{68}	28.24	-19.09	-1.35
101	c_{69}	0.40	-2.09	-0.12
102	c_{610}	63.34	-33.79	-2.55
103	c_{611}	11.39	-4.89	-0.40
104	c_{612}	-61.86	37.22	2.72
105	c_{612}	7.62	-7.68	-0.49
106	c_{614}	46.65	-14.64	-1.33
107	c_{615}	-22.43	9.15	0.76
108	c_{616}	-77.97	37.53	2.92

* To be continued *

TABLE 5.1: (continued)

i	Term	Polynomial Coefficients		
		$RSM_Z/10^{11}$	$RSM_X/10^{10}$	$RSM_R/10^9$
109	c_{78}	-46.77	27.55	2.02
110	c_{79}	1.33	2.35	0.11
111	c_{710}	-4.60	2.26	0.18
112	c_{711}	-32.09	25.87	1.76
113	c_{712}	-8.38	10.67	0.65
114	c_{713}	3.57	-10.36	-0.59
115	c_{714}	85.93	-55.00	-3.94
116	c_{715}	-46.71	32.17	2.27
117	c_{716}	-15.93	12.72	0.86
118	c_{89}	-96.89	56.30	4.15
119	c_{810}	61.61	-34.69	-2.57
120	c_{811}	80.81	-44.76	-3.33
121	c_{812}	-19.81	13.47	0.95
122	c_{813}	-55.54	27.41	2.12
123	c_{814}	59.10	-35.84	-2.60
124	c_{815}	-10.98	6.07	0.45
125	c_{816}	51.73	-28.89	-2.15
126	c_{910}	-18.44	2.51	0.35
127	c_{911}	38.12	-24.12	-1.73
128	c_{912}	-58.11	31.17	2.35
129	c_{913}	-18.94	8.19	0.66
130	c_{914}	4.43	-1.31	-0.13
131	c_{915}	6.35	-5.24	-0.35

* To be continued *

TABLE 5.1: (continued)

i	Term	Polynomial Coefficients		
		$RSM_Z/10^{11}$	$RSM_X/10^{10}$	$RSM_R/10^9$
132	c_{916}	40.35	-24.23	-1.78
133	c_{1011}	6.25	0.94	-0.02
134	c_{1012}	-32.20	17.05	1.29
135	c_{1013}	44.91	-23.08	-1.76
136	c_{1014}	16.04	-9.50	-0.70
137	c_{1015}	-15.13	6.17	0.50
138	c_{1016}	-26.04	13.20	1.02
139	c_{1112}	41.13	-21.52	-1.63
140	c_{1113}	38.49	-13.15	-1.15
141	c_{1114}	5.20	-1.30	-0.13
142	c_{1115}	-4.35	5.22	0.33
143	c_{1116}	23.46	-11.81	-0.90
144	c_{1213}	40.19	-23.64	-1.74
145	c_{1214}	-32.49	31.43	2.06
146	c_{1215}	-60.18	31.99	2.41
147	c_{1216}	5.42	-3.65	-0.26
148	c_{1314}	-25.02	15.51	1.12
149	c_{1315}	22.90	-13.02	-0.97
150	c_{1316}	-84.23	49.39	3.62
151	c_{1415}	-1.34	-0.49	0.00
152	c_{1416}	-36.51	16.02	1.28
153	c_{1516}	-40.56	20.14	1.55
154	d_{11}	7.94	-3.63	-0.28

* To be continued *

TABLE 5.1: (continued)

i	**Term**	**Polynomial Coefficients**		
		$RSM_Z/10^{11}$	$RSM_X/10^{10}$	$RSM_R/10^9$
155	d_{22}	-60.09	30.60	2.33
156	d_{33}	-18.80	5.49	0.50
157	d_{44}	-2.84	1.93	0.14
158	d_{55}	-2.77	3.51	0.22
159	d_{66}	-98.33	57.67	4.23
160	d_{77}	38.00	-16.45	-1.32
161	d_{88}	-2.82	-2.87	-0.13
162	d_{99}	108.96	-61.83	-4.57
163	d_{1010}	-181.90	94.06	7.13
164	d_{1111}	144.26	-76.36	-5.76
165	d_{1212}	-38.02	19.02	1.46
166	d_{1313}	1.21	0.03	-0.01
167	d_{1414}	73.76	-38.61	-2.92
168	d_{1515}	-45.76	20.64	1.64
169	d_{1616}	43.23	-23.28	-1.76

Appendix 2

TABLE 5.2: Design variables for N1-N7

i	N1 model				N2 model			
	a_i	b_i	c_i	d_i	a_i	b_i	c_i	d_i
1	0.0028	0.0484	0.0010	-0.0062	0.0024	0.0544	0.0010	-0.0063
2	0.0380	0.1929	0.0008	0.0103	0.0336	0.1783	0.0008	0.0083
3	0.4851	0.0341	-0.1614	-0.1155	0.4782	0.0491	-0.1972	-0.0914
4	-0.2552	0.1150	0.1298	0.0712	-0.2535	0.1248	0.1390	0.0521
i	N3 model				N4 model			
	a_i	b_i	c_i	d_i	a_i	b_i	c_i	d_i
1	0.0023	0.0383	0.0011	-0.0052	0.0023	0.0601	0.0008	-0.0064
2	0.0435	0.1775	0.0007	0.0122	0.0331	0.2163	0.0008	0.0129
3	0.4694	0.0457	-0.1638	-0.1477	0.3515	0.0424	-0.2046	-0.1132
4	-0.2565	0.1076	0.1218	0.0604	-0.2038	0.1424	0.1435	0.0588
i	N5 model				N6 model			
	a_i	b_i	c_i	d_i	a_i	b_i	c_i	d_i
1	0.0023	0.0601	0.0008	-0.0064	0.0031	0.0440	0.0010	-0.0060
2	0.0331	0.2163	0.0008	0.0129	0.0310	0.1842	0.0006	0.0121
3	0.3515	0.0424	-0.2046	-0.1132	0.3923	0.0436	-0.1546	-0.1140
4	-0.2038	0.1424	0.1435	0.0588	-0.2374	0.1583	0.1382	0.0575
i	N7 model							
	a_i	b_i	c_i	d_i				
1	0.0025	0.0450	0.0010	-0.0051				
2	0.0414	0.1969	0.0007	0.0118				
3	0.3010	0.0410	-0.1502	-0.1104				
4	-0.2486	0.1076	0.1485	0.0509				